European Journal of Applied Mathematics (2025), 1–27
doi:10.1017/S0956792525100247

CAMBRIDGE UNIVERSITY PRESS

PAPER

Ageing and mortality of persons with HIV: a novel data-driven approach

Alex Viguerie[1] and Elisa Iacomini[2]

[1]Department of Pure and Applied Sciences, Università degli studi di Urbino Carlo Bo, Urbino, Italy
[2]Department of Environmental and Prevention Sciences, Università degli studi di Ferrara, Ferrara, Italy
Corresponding author: Elisa Iacomini; Email: elisa.iacomini@unife.it

Received: 17 April 2025; **Revised:** 17 October 2025; **Accepted:** 17 October 2025

Keywords: HIV; population-structured models; inverse ensemble Kalman filter; dynamic mode decomposition

2020 Mathematics Subject Classification: Primary - 92D25, Secondary - 47N60, 37M99, 60G35

Abstract

Due to the widespread availability of effective antiretroviral therapy regimens, average lifespans of persons with HIV (PWH) in the United States have increased significantly in recent decades. In turn, the demographic profile of PWH has shifted. Older persons comprise an ever-increasing percentage of PWH, with this percentage expected to further increase in the coming years. This has profound implications for HIV treatment and care, as significant resources are required not only to manage HIV itself, but also associated age-related comorbidities and health conditions that occur in ageing PWH. Effective management of these challenges in the coming years requires accurate modelling of the PWH age structure. In the present work, we introduce several novel mathematical approaches related to this problem. We present a workflow combining a PDE model for the PWH population age structure, where publicly available HIV surveillance data are assimilated using the Ensemble Kalman Inversion algorithm. This procedure allows us to rigorously reconstruct the age-dependent mortality trends for PWH over the last several decades. To project future trends, we introduce and analyse a novel variant of the dynamic mode decomposition (DMD), nonnegative DMD. We show that nonnegative DMD provides physically consistent projections of mortality and HIV diagnosis while remaining purely data-driven, and not requiring additional assumptions. We then combine these elements to provide forecasts for future trends in PWDH mortality and demographic evolution in the coming years.

1. Introduction

In recent decades, the life expectancy of individuals living with HIV, particularly in industrialised countries, has increased significantly, largely due to advancements in antiretroviral therapy (ART) [10, 72]. ART has transformed HIV from a fatal disease into a manageable chronic condition, allowing many persons with HIV (PWH) to live lifespans nearly commensurate with the general population [31, 55, 72]. As a result, the demographic profile of persons with diagnosed HIV (PWDH) in the United States has shifted. As shown in Figure 1, persons aged 55 and older have gone from approximately 16% of the PWDH population in 2008 to nearly 45% in 2022 [26]. Such a drastic demographic shift presents new challenges in the fight against HIV, as long-term management of chronic HIV infection will require an increasing share of resources.

The growing population of older PWDH requires the healthcare system to address not only the ongoing management of HIV itself, but also, increasingly, comorbidities and age-related conditions that arise as this population ages. These include cardiovascular disease, diabetes, osteoporosis, and certain cancers, which occur at higher levels, and at younger ages, among PWH as compared to the general population [7, 8, 16, 27, 59, 61, 64, 65]. Older PWH also may suffer from cognitive and functional impairment

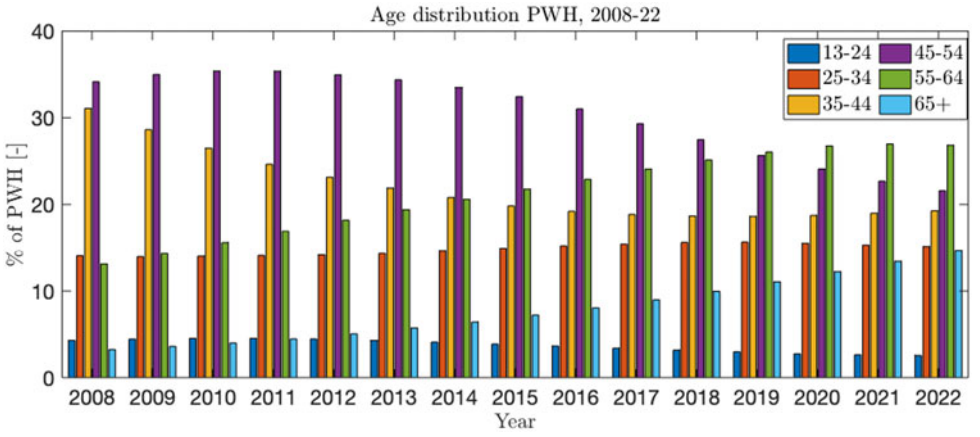

Figure 1. *Age distribution of the diagnosed PWH population in the United States over the years 2008 – 22.*

[56, 60]. In addition, the high burden of health comorbidities leads to high levels of polypharmacy among older PWDH [69]. Finally, although ART has significantly increased overall lifespan among PWDH, ART itself is associated with health complications arising from long-term use [13, 30, 69]. As a result, healthcare providers must adapt their approaches and strategies to encompass a broader spectrum of health issues among PWH [16, 42].

Given the changing landscape of HIV care, the focus of public health strategies must also evolve. Prevention efforts now must include the mitigation of health complications associated with HIV in older adults, long-term HIV infection and long-term ART use among PWDH [16, 42], necessitating a comprehensive approach that integrates HIV care with general healthcare for chronic disease prevention and management [16, 42, 61]. Effective strategies will be crucial to maintain the health and quality of life of the ageing PWDH, ensuring that the progress made in extending life expectancy is not undermined by the rise of preventable chronic conditions, and that increased life-years are not accompanied by decreased life quality. Furthermore, despite decreases in new HIV infections and diagnoses in recent years, improved life expectancy among PWDH has led to a significant increase in the PDWH population as a whole in the United States and other high-income countries [25, 63], compounding ageing-related difficulties, as HIV care must be allocated across a large, and increasing, population.

To help address these challenges, the development of accurate mathematical models capable of providing reliable projections for the PWDH age structure in coming years is an important priority in HIV policy research. Such models can play a fundamental role in the planning and evaluation of intervention strategies and the allocation of valuable HIV treatment and prevention services. Recent work on this topic includes [70], which applied a compartment model for demographic projections, and [5, 35], which used an agent-based model to project how demographic changes in the US PWDH population may affect the burden of comorbidities. A particularly important component of these models is their ability to accurately characterise age-dependent PWDH mortality rates, and furthermore, how they may change in coming years. This arguably forms the foundation of such models, as the overall cost of HIV-related care depends most heavily on total PWDH person-years.

Given the importance of the topic, in the present work, we seek to estimate how the age-dependent mortality rates for PWDH in the US have changed in recent years in a mathematically rigorous manner, and furthermore, extrapolate from these data to project future such changes. To the authors' knowledge, no such study has been undertaken, certainly not to describe changes in mortality at the age- and time-continuous level. To accomplish this task, we employ a data assimilation approach, in which age-discrete HIV surveillance data are integrated into a partial differential equation (PDE) model via an inverse ensemble Kalman filter (EnKF) to reconstruct the time evolution of age-dependent PWDH mortality

https://doi.org/10.1017/S0956792525100247 Published online by Cambridge University Press

since 2009. To project future trends in age-dependent mortality based on our reconstructions, we develop and apply a novel variant of dynamic mode decomposition (DMD), nonnegative DMD. By incorporating these data into our PDE model, we provide a forecast PWDH age structure, annual HIV diagnoses, and annual PWDH deaths in the United States over the coming years.

To reconstruct the evolution of age-dependent PWDH mortality rates in recent years, we employ the Ensemble Kalman Inversion (EKI). The EKI is an adaptation of the EnKF, a powerful tool for estimating the state of a dynamical system by iteratively refining predictions based on noisy observations. Originally introduced in the 1990s [22], the EnKF has gained widespread use due to its ability to fuse model predictions with measurement data. Ensemble Kalman filtering has been employed to enhance the accuracy of solutions in diverse applications, including oceanography [23], reservoir modelling [1], weather forecasting [37], milling process [68], geophysical applications [39], physics [54] and machine learning [47, 80]. In public health, the EnKF was recently used to forecast heroin overdose deaths [11]. The EKI is a modified version of the EnKF designed for inverse problems, wherein underlying model parameters are estimated given a time-series of observations corresponding to model states [32–34, 66]. The EKI is attractive computationally, as it does not require the computation of derivatives of the underlying model, as well as mathematically, as it allows for provable convergence results [34, 66].

To project future trends from the reconstructed mortality data, we introduce a novel modification of the DMD, nonnegative DMD. DMD is a scientific machine learning (SciML) technique that extracts the most relevant dynamical structures existent in time-series data using a purely data-driven approach, with applications ranging from short-time future estimates to control, modal analysis and dimension reduction [48]. DMD has been deployed in a wide range of scientific and engineering applications such as biomechanics [75], oncology [75] epidemiology [6, 62, 74], climate modelling [49], aeroelasticity [24], additive manufacturing [74], urban mobility [3] and the modelling and simulation of batteries [4]. The authors are not aware of any work using DMD to forecast the evolution of mortality rates, or similar quantities. In general, however, standard DMD fail to respect non-negativity when used for forecasting beyond the training period, even when the underlying training data are nonnegative [71, 74]. This makes DMD in its original formulation potentially unsuitable for forecasting nonnegative quantities, such as mortality rates, and as such must be modified accordingly.

The article is outlined as follows. In the methods section, we provide a high-level description of the mathematical model and the EnKF method. We then introduce the proposed novel variant of DMD, nonnegative DMD, discuss its numerical solution and establish some of its basic mathematical properties. We then present the results of our analyses. We first present the reconstructions of age-dependent PWDH mortality curves over previous years. We then use nonnegative DMD to obtain projections of future mortality rates, and apply these rates in our underlying PDE model in order to provide projections for age-dependent PWDH prevalence and mortality through 2030. We then provide a detailed discussion of the implications of our findings and conclude by discussing possible future directions to extend this research.

2. Methods

2.1. Mathematical model

We consider an age-structured PDE model for the population $u(a, t)$, which gives the size of the PWDH population u aged a at a time t. Models of this type allow for a precise description of age that is difficult to achieve with discrete age-structuring (e.g. a compartmental approach), particularly given age- and time-scales of the data do not coincide. Indeed, the surveillance data are reported annually, however, the reported age groups are 5-or 10-year ranges. The basic equations read:

$$\frac{\partial u}{\partial t} + \frac{\partial u}{\partial a} = -\mu(a,t)u + \lambda(a,t) \quad \text{for } t_0 < t \le t_{end},\ 0 \le a < \infty,$$
$$u(a,0) = u_0(a) \quad \text{at } t = t_0, \quad u(0,t) = g(t), \tag{2.1}$$

https://doi.org/10.1017/S0956792525100247 Published online by Cambridge University Press

where $\mu(a,t) \geq 0$ is the age- and time-dependent mortality rate, $u_0 \geq 0$ is the age-distribution of the PWDH population at the initial time, and $\lambda(a,t) \geq 0$ gives the number of new HIV diagnoses of persons aged a at a time t, and is known from data.

The inflow condition $g(t) \geq 0$ defines new births, and may be time- and/or state-dependent in general. In the present, however, we assume $g(t) = 0$, for several reasons. First, levels of perinatal HIV in the US are very low [50]. Second, publicly available HIV surveillance data in the US does not include persons younger than 13 years of age [25]. Finally, the method of generating continuous age-distributions from discrete age-bins available from surveillance data (discussed in section 2.2), used to generate $u_0(a)$ and $\lambda(a,t)$, ensures $u(a,t) > 0$ and remains smooth for all $a > 0$ throughout the simulation period.

In practice, we solve (2.1) numerically, considering a bounded age domain $0 \leq a \leq 101$. We employ a second-order backward differentiation (BDF2) scheme throughout the age domain, assuming physically consistent 'ghost node' values of $a^t_{-1} = a^t_{-2} = 0$ for all t. For the time discretisation, we use Heun's method to solve the first time step, and BDF2 for the remaining time steps. Models of this type are common in many applications in the natural and social sciences, and we refer the reader to [57] for a presentation of these models and [53] for an extensive discussion of more complex extensions.

Denote the domain of $u(\cdot,t)$, the set of admissible human ages, as $\mathbb{A} = \mathbb{R}^+ = [0,\ \infty)$, endowed with a σ-algebra $\mathfrak{B}$ and nonnegative measure $\nu(A)$. In the following, we use $u(a,t)$ to denote a generic solution of (2.1) and provide the following positivity result:

Theorem 1. *If $u_0 \geq 0$ for all a and $\mu \geq 0,\ \lambda \geq 0$ for all (a,t), then $u(a,t) \geq 0$ for all (a,t).*

Proof. *Since the age a advances in sync with time, we can consider the characteristic curve $a(t) = a_0 + t$ for some fixed a_0, and note that $da/dt = 1$. Along the characteristic, we can rewrite (2.1) in terms of a function $v(t)$, depending only on t:*

$$v(t) := u(a(t),t) = u(a_0 + t, t). \tag{2.2}$$

Differentiating with respect to t gives:

$$\frac{dv}{dt} = \frac{\partial u}{\partial t} + \frac{\partial u}{\partial a}\frac{d}{dt}[a_0 + t] = \frac{\partial u}{\partial t}(a_0 + t,\ t) + \frac{\partial u}{\partial a}(a_0 + t,\ t). \tag{2.3}$$

where the last equation on the right hand side follows from $da/dt = 1$. From (2.2), (2.3) along the characteristic (2.1) reduces to the ordinary differential equation:

$$\frac{dv}{dt} = -\mu(a_0 + t, t)v(t) + \lambda(a_0 + t, t). \tag{2.4}$$

Re-arranging, multiplying by the integrating factor $e^{\int_0^t \mu(a_0+\tau,\tau)d\tau}$, and integrating from 0 to t:

$$v(t)e^{\int_0^t \mu(a_0+\tau,\tau)d\tau} = v(0) + \int_0^t \lambda(a_0 + \xi, \xi)e^{\int_0^\xi \mu(a_0+\tau,\tau)d\tau}d\xi. \tag{2.5}$$

Recalling that $v(0) = u_0(a_0)$:

$$u(a_0 + t, t) = e^{-\int_0^t \mu(a_0+\tau,\tau)d\tau}\left(u_0(a_0) + \int_0^t \lambda(a_0 + \xi, \xi)e^{\int_0^\xi \mu(a_0+\tau,\tau)d\tau}d\xi\right). \tag{2.6}$$

From our assumptions on $\mu,\ u_0,\ \lambda$, all the terms on the right-hand side are nonnegative, and hence:

$$u(a_0 + t, t) \geq 0\ \ \forall t. \tag{2.7}$$

Furthermore, since a_0 was arbitrary, (2.7) holds for any $a_0 \geq 0$, implying:

$$u(a,t) \geq 0\ \ \forall (a,t), \tag{2.8}$$

as was to be shown. □

https://doi.org/10.1017/S0956792525100247 Published online by Cambridge University Press

2.2. Ensemble Kalman inversion

The EKI is a computational technique that extends the principles of the Kalman filter to solve inverse problems by utilising an ensemble of model realizations. By iteratively updating this ensemble with observational data, which are assumed to be affected by noise, EKI effectively estimates unknown parameters and reduces uncertainty, making it particularly suitable for high-dimensional and nonlinear inverse problems [33, 34, 66].

Here, we describe the EKI procedure applied in the current work. In order to do this, let us introduce the notation we will use in the following:

- The overline symbol $\bar{\cdot}$ denotes an averaged quantity.
- $u(a, t)$ denotes the age-distribution of the PWDH population in time.
- $\boldsymbol{\mu}(a, t)$ is our unknown; in this case, it defines the time- and age-dependent mortality curve.
- Γ is the matrix of the covariance of the noise, which is assumed to be known.
- $\mathscr{G}(\cdot)$ is our output of the total annual PWDH deaths in each age bracket, calculated from the population state u and mortality curve μ.
- n_{kf} is the number of Kalman filtering steps.
- $A(\boldsymbol{\mu}, \lambda, u)$ is the operator which advances population age distribution Δt units in time for a given $\boldsymbol{\mu}(a, t)$ and $\lambda(a, t)$ according to the system dynamics defined by (2.1):

$$u(a, t + \Delta t) = A\left(\boldsymbol{\mu}(a, t), \lambda(a, t), u(a, t - s\Delta t)|_{s=1}^{S}\right) u(a, t). \tag{2.9}$$

  Note: A may depend on up to S additional past time steps in general, according to the time-stepping scheme employed.

For the sake of readibility, we hereafter write $\boldsymbol{\mu}(a, t)$, $u(a, t)$, and $\lambda(a, t)$, respectively, as $\boldsymbol{\mu}_t$, u_t, and λ_t, with the dependence of each quantity on age a understood if not explicitly denoted. We seek to use the EKI to estimate the time- and age-dependent mortality curve $\boldsymbol{\mu}_t$, which is not observable directly, by incorporating information from the model (2.1) and surveillance data. The estimation of $\boldsymbol{\mu}_t$ relies on the current age distribution P_t, calculated from the (2.1), and the age-bracketed annual mortality data y_t, available from surveillance data [26]. To ensure regularity in our estimate, we do not estimate $\boldsymbol{\mu}_t$ at each age individually, but compute its value at ages 1, 10, 22, 32, 42, 52, 57, 62, 67, 72, 77, 82, 95, 101. We then consider the full curve $\boldsymbol{\mu}_t$ as the piecewise cubic Hermite interpolating polynomial through these points. We note that we performed a sensitivity analysis to the choice of interpolation points, and found that the effect on the overall reconstruction was not large, provided that there are sufficiently many points across all age ranges.

We begin by initialising an ensemble of mortality curves at $\boldsymbol{\mu}_{t,j}^1$ for $j = 1, \ldots, J$ at $t = 2009$, by sampling from the distribution of the mortality rate of the general (non-PWH) population $\boldsymbol{\mu}_0$. The superscript number refers to the current filter step, further clarified in the following. We assume a multivariate normal distribution with mean $\boldsymbol{\mu}_0$ and covariance $\mathrm{diag}(\boldsymbol{\mu}_0^2)$, the component-wise square.

Similarly, we also initialise an ensemble of population age structures $P_{t_0,j}$ for $j = 1, 2, \ldots, J$ at the initial time $t_0 = 2009$, which serve as the initial conditions for (2.1). Each $P_{t_0,j}$ is generated from surveillance data for the diagnosed PWDH population at year-end 2008 [26]. These data are stratified into age brackets: 13 – 24, 25 – 34, 35 – 44, 45 – 54, 55 – 59, 60 – 64, 65 – 69, 70 – 74, 75 – 79, 80 – 84 and 85 +. We define each $P_{t,j}^1$ such that the overall number of PWDH in each age bracket is equal to the surveillance data, while the distribution of PWDH *within* each age bracket are defined with a uniform sample. For each calendar year $t_i = 2009 - 22,\ i = 1, 2, \ldots$ during the simulation, we follow an identical procedure using the age-bracketed annual new HIV diagnosis data from [26] to define an ensemble $\lambda_{t_i,j}$, $j = 1, 2, \ldots, J$ for new entries in the model (2.1).

Assume that (2.1) is discretised time with time step $\Delta t = 1/m,\ m \in \mathbb{N}$, such that each year is divided into m time-steps. For each simulated calendar year t_i, we perform n_{kf} inverse Kalman Filtering steps. The procedure is given in Algorithm (1). In a given year, we perform n_{kf} filtering steps. At the nn-th

https://doi.org/10.1017/S0956792525100247 Published online by Cambridge University Press

Algorithm 1 Algorithm with fixed number of filter steps for the model $\mathscr{G}$

Initialise state ensemble $u_{t_0,j}$

Initialise measurement noise: $Q = \text{diag}(\text{Var}(\mathscr{G}(u_{t_0}, \boldsymbol{\mu}_0))$, a diagonal matrix consisting of the variance in observed deaths in each age group for the general-population mortality $\boldsymbol{\mu}_0$ over the initial state ensemble u_{t_0}.

Initialise the mortality curve ensemble $\boldsymbol{\mu}_{t_0,j}^{n_{kf}} \sim N(\boldsymbol{\mu}_0,\ \text{diag}(\boldsymbol{\mu}_0^2))$, with $j = 1,\ 2,\ \ldots\ldots,J$, where $\boldsymbol{\mu}_0^2$ is interpreted as the element-wise square, and $n_{kf} > 0$ the number of optimisation steps

Set $n = 0$, $t_1 = 2009$

for t_i=2009:2022 **do**

  Generate ensemble of annual new diagnoses $\lambda_{t_i,j}$;

  Set $\boldsymbol{\mu}_{t_i,j}^1 = \boldsymbol{\mu}_{t_{i-1},j}^{n_{kf}}$;

  for nn=1:n_{kf} **do**

    Set $\mathscr{G}(u_j, \boldsymbol{\mu}_{t_i,j}^{nn}) = \mathbf{0}$;

    for $k = 1{:}m$ **do**

      Advance the population structure ensemble and age-structured mortality output:

$$u_{t_i+k\Delta t,j} = A(\boldsymbol{\mu}_{t_i,j}^{nn}, \lambda_{t_i,j}, u_{t_i+(k-s)\Delta t,j}|_{s=2}^{S})u_{t_i+(k-1)\Delta t,j};$$

$$\mathscr{G}(u_j, \boldsymbol{\mu}_{t_i,j}^{nn}) = \mathscr{G}(u_j, \boldsymbol{\mu}_{t_i,j}^{nn}) + \Delta t\, \text{diag}(\boldsymbol{\mu}_{t_i,j}^{nn})\ \text{diag}(\boldsymbol{\mu}_{t_i,j}^{nn})\, u_{t_i+k\Delta t,j};$$

    end for

    $\bar{\boldsymbol{\mu}}^{nn} = \frac{1}{J}\sum_{j=1}^{J} \boldsymbol{\mu}_{t_i,j}^{nn}$

    $\overline{\mathscr{G}}^{nn} = \frac{1}{J}\sum_{j=1}^{J} \mathscr{G}(u_j, \boldsymbol{\mu}_{t_i,j}^{nn})$

    $\boldsymbol{\eta} \sim \mathcal{N}(0, Q)$

    Solve the EnKF procedure:

$$C(\boldsymbol{\mu}^{nn}) = \tfrac{1}{J}\sum_{j=1}^{J} (\boldsymbol{\mu}_j^{nn} - \overline{\boldsymbol{\mu}}^{nn}) \otimes (\mathscr{G}(u_j, \boldsymbol{\mu}_j^{nn}) - \overline{\mathscr{G}}^{nn})$$

$$D(\boldsymbol{\mu}^{nn}) = \tfrac{1}{J}\sum_{j=1}^{J} (\mathscr{G}(u_j, \boldsymbol{\mu}_j^{nn}) - \overline{\mathscr{G}}^{nn}) \otimes (\mathscr{G}(u_j, \boldsymbol{\mu}_j^{nn}) - \overline{\mathscr{G}}^{nn}) \qquad \text{(EnKF)}$$

$$\boldsymbol{\mu}_j^{nn+1} = \boldsymbol{\mu}_j^{nn} + C(\boldsymbol{\mu}^{nn})\left(D(\boldsymbol{\mu}^{nn}) + \Gamma^{-1}\right)^{-1}\left(y_{t_i} + \boldsymbol{\eta} - \mathscr{G}(u_j, \boldsymbol{\mu}_j^{nn})\right)$$

  end for

end for

filtering step, we first advance the P_j^{nn} following (2.1) by solving the model over m time-steps, using $\lambda_{t_i,j}$ and the mortality curve $\boldsymbol{\mu}_{t_i,j}^{nn}$. Note that we must keep a running update of the simulated age-bracketed mortality $\mathscr{G}(P_j^{nn}, \boldsymbol{\mu}_{t_i,j}^{nn})$ at each time step, so that an end-of-year total is available.

If nn is less than the total number of filter steps n_{kf}, we use the calculated $\mathscr{G}(P_j^{nn}, \boldsymbol{\mu}_{t_i,j}^{nn})$ and the surveillance mortality data y_{t_i} to obtain the updated mortality curve $\boldsymbol{\mu}_{t_i,j}^{nn+1}$. We then simulate the model for the year t_i again, using with the updated $\boldsymbol{\mu}_{t_i,j}^{nn+1}$. If $nn = n_{kf}$, we advance to year t_{i+1}, setting $\boldsymbol{\mu}_{t_{i+1},j}^{1} = \boldsymbol{\mu}_{t_i,j}^{n_{kf}}$ and generating $\lambda_{t_{i+1},j}$ from the surveillance data for year t_{i+1}. Note that the solution of the EnKF procedure is given by the mean of the ensemble at the step n_{kf} for each year.

Remark. Note that, as (2.1) must be solved n_{kf} times in each year, we must keep values of P_j from the preceding year in order to repeatedly solve the first time-step of the current year. The exact number of time-step(s) to be saved depends on the specific time-stepping scheme used. As we used BDF2 in the current work, we kept the last two time-steps from the n_{kf}-th filtering step of the previous year.

https://doi.org/10.1017/S0956792525100247 Published online by Cambridge University Press

2.3. Nonnegative DMD

In the present work, we introduce a novel variant of DMD, nonnegative DMD, and use it to extrapolate the evolution of the age-dependent mortality rates (calculated using the EKI) and the age structure of new HIV diagnoses (estimated from surveillance data) through the year 2030. In the following, we will provide a brief introduction to the standard DMD algorithm, then we will introduce the nonnegative DMD algorithm, and provide some information regarding its calculation.

2.3.1. Standard DMD

In this subsection, we provide a brief description of DMD. For the purposes of simplicity and exposition, we restrict our discussion to the original formulation of DMD as proposed in [67]. We remark that this is a vast topic of research, and refer the reader to [48] for a more comprehensive treatment of DMD. Suppose, we have time series consisting of n snapshots:

$$\left\{x_i\right\}_{i=1}^{n}, \qquad x_i \in \mathbb{R}^m \quad \forall i. \tag{2.10}$$

We arrange these snapshots into two $m \times n-1$ matrices X_1, X_2 column-wise as follows:

$$X_1 = \begin{bmatrix} | & | & & | \\ x_1 & x_2 & \dots & x_{n-1} \\ | & | & & | \end{bmatrix} X_2 = \begin{bmatrix} | & | & & | \\ x_2 & x_3 & \dots & x_n \\ | & | & & | \end{bmatrix}. \tag{2.11}$$

DMD seeks to reconstruct the operator A mapping X_1 to X_2, that is:

$$AX_1 = X_2, \tag{2.12}$$

which can be obtained as [67]:

$$A = X_2 \left(X_1\right)^{\dagger}, \tag{2.13}$$

where $X_1^{\dagger}$ is the Moore-Penrose pseudoinverse of X_1 (see e.g. [28]). This formulation of A solves the minimisation problem:

$$\arg\min_{A} \|AX_1 - X_2\|_F, \tag{2.14}$$

with $\|\cdot\|_F$ denoting the Frobenius norm [48]. Note that, in practice, A can be large and dense, and is not typically computed directly as (2.13). Instead, algorithms which efficiently compute lower-rank approximations of A can be leveraged to avoid ever forming A explicitly (see e.g. [48, 67, 75]).

2.3.2. Nonnegative DMD algorithm

Being a completely data-driven algorithm, DMD, particularly when extrapolated past the training interval, will not necessarily respect the physics of the underlying systems. For example, in [4], it was demonstrated that standard DMD can fail to predict periodic limit cycles. Similarly, in [74], it was shown that DMD, when formulated as (2.13) (or with a lower-rank approximation), will conserve the mass of a mass-conservative system (assuming the data is also mass-conservative), even projected out in time; however, other key physical properties, in particular nonnegativity, were not preserved in the extrapolations.

In the present work, we employ DMD to project two strictly nonnegative physical quantities: future HIV diagnoses and future age-dependent mortality rates among PWH. While standard DMD reliably reproduces the training data in both instances, attempting to extrapolate beyond the training interval results in negative, oscillatory reconstructions, even over short projection windows (1–2 years).

In order to guarantee $(A^n x)_i \geq 0, \ \forall\, i,\ n$, assuming a nonnegative x, it is enough to guarantee that the matrix A itself is nonnegative. The most obvious solution would be to find A as in (2.13), and then use

https://doi.org/10.1017/S0956792525100247 Published online by Cambridge University Press

nonnegative matrix factorisation to replace A with an approximate nonnegative version $A \approx \widehat{A} = MN$, that is:

$$\arg\min_{\widehat{A}=MN} \|MN - X_2(X_1)^\dagger\|_F, \quad M_{i,j}, N_{i,j} \geq 0 \ \forall i, j. \tag{2.15}$$

However, our attempts in this direction were unsuccessful, and approximations of A obtained in this way did not provide useful forecasts; we will elaborate further later in the text.

As $\{x\}_{i=1}^n > 0$ element-wise for all i, we also attempted to define:

$$\widetilde{X}_1 = \log(X_1), \ \widetilde{X}_2 = \log(X_2), \ \widetilde{A} = \widetilde{X}_2(\widetilde{X}_1)^\dagger, \tag{2.16}$$

and proceeding as:

$$x_{i+1} = \exp\left(\widetilde{A}\log(x_i)\right). \tag{2.17}$$

Note that the logarithm and exponential functions in (2.16), (2.17) refer to the elementwise operations. While the x_i x_i obtained in this manner remained nonnegative, and accurately reconstructed the training period, extrapolation beyond the training period resulted in oscillatory, nonphysical solutions, even for just a single time-step, making this approach unsuitable for forecasting, at least for the problems studied herein.

To understand the poor performance of the log-transform approach, note that the operator $\widetilde{A}$ minimises:

$$\sum_{i=1}^{n} \|\widetilde{A}\log(x_i) - \log(x_{i+1})\|_2^2, \tag{2.18}$$

which is not equivalent to minimising:

$$\sum_{i=1}^{n} \|Ax_i - x_{i+1}\|_2^2 \tag{2.19}$$

in general. Furthermore, given the lack of specific structure on $\widetilde{A}$, large complex eigenvalues are common. In log-space, these result in rotations:

$$\log x_{i+1} = \sum_j \widetilde{A}_{i,j} \log x_j. \tag{2.20}$$

However, upon exponentiation, (2.20) becomes:

$$x_{i+1} = \prod_j x_j^{\widetilde{A}_{i,j}}, \tag{2.21}$$

and the rotations in log-space result in spurious, nonphysical oscillations in linear space.

Instead, we formulate nonnegative DMD as the following:

Definition. *Let $X \in \mathbb{R}^{m\times n}$ and let X_1, X_2 be snapshot matrices as defined in (2.11). We define the nonnegative DMD as the operator A satisfying:*

$$\arg\min_A \|AX_1 - X_2\|_F, \quad A_{i,j} \geq 0 \ \forall i, j. \tag{2.22}$$

In general, the solutions to (2.15) and (2.22) do not coincide. Let $A_{\mathrm{LS}} := X_2X_1^\dagger$ be the unconstrained DMD fit (2.13). Noting that:

$$A_{LS}X_1 = X_2 \tag{2.23}$$

https://doi.org/10.1017/S0956792525100247 Published online by Cambridge University Press

and using the normal equations $A_{\mathrm{LS}}X_1X_1^T = X_2X_1^T$, we have for any A:

$$\begin{aligned}\|AX_1 - X_2\|_F^2 &= \|(A - A_{\mathrm{LS}})X_1 + (A_{\mathrm{LS}}X_1 - X_2)\|_F^2 \\ &= \|(A - A_{\mathrm{LS}})X_1\|_F^2 \\ &\quad + 2\underbrace{\langle (A - A_{\mathrm{LS}})X_1,\, A_{\mathrm{LS}}X_1 - X_2\rangle_F}_{=0} + \|A_{\mathrm{LS}}X_1 - X_2\|_F^2 \\ &= \|(A - A_{\mathrm{LS}})X_1\|_F^2 + \|A_{\mathrm{LS}}X_1 - X_2\|_F^2. \end{aligned} \tag{2.24}$$

Note that the second term on the right-hand side above is independent of A. Since $\|(A - A_{\mathrm{LS}})X_1\|_F^2 = \mathrm{tr}\big((A - A_{\mathrm{LS}})X_1X_1^T(A - A_{\mathrm{LS}})^T\big)$, problem (2.22) is the *metric projection* of A_{LS} onto the elementwise nonnegative cone $\{A\colon A \geq 0\}$ in the weighted inner product:

$$\langle U, V\rangle_{X_1} := \mathrm{tr}(U\, X_1X_1^T\, V^T),$$

By contrast, (2.15) minimises

$$\min_{M,N\geq 0} \|MN - A_{\mathrm{LS}}\|_F^2,$$

that is, a projection of A_{LS} onto the set

$$\mathscr{S}_r := \{MN\colon M \in \mathbb{R}_+^{m\times r},\ N \in \mathbb{R}_+^{r\times m}\}$$

under the standard Euclidean metric.

These two projections differ because the geometry induced by the data through $X_1X_1^T$ is not the Euclidean one. They coincide only in degenerate cases (e.g. $G \propto I$ or $A_{\mathrm{LS}} \geq 0$); and, for (2.15), with r large enough to represent the same feasible A. Practically, (2.15) fits A_{LS} in matrix space, ignoring how A acts on X_1, whereas (2.22) enforces nonnegativity directly on the *forecasting loss* $\|AX_1 - X_2\|_F$, the quantity that matters for prediction.

The computation of (2.22) is nontrivial. Note that well-known algorithms exist to solve the related matrix-vector *nonnegative least squares* (NNLS) problem: [52]:

$$\arg\min_x \|Ax - b\|_2 \quad x_j \geq 0\ \ \forall j. \tag{2.25}$$

Problems related to (2.22), in which one searches for a nonnegative matrix, have been studied in [40, 41, 58, 73]. We remark that, in each of these cases, it is assumed that one has access to the matrix A and is attempting to find X_1, that is solving:

$$\arg\min_{X_1} \|AX_1 - X_2\|_F, \quad X_{1_{i,j}} \geq 0\ \ \forall i, j. \tag{2.26}$$

The DMD problem is the opposite, since X_1 is known from the data and A is our unknown. However, recalling that $\|M\|_F = \|M^T\|_F$ [28] for any matrix M, the transposed problem:

$$\arg\min_{A^T} \|X_1^TA^T - X_2^T\|_F, \quad A_{i,j}^T \geq 0\ \ \forall i, j \tag{2.27}$$

is equivalent to (2.26). Note that:

$$\|X_1^TA^T - X_2^T\|_F^2 = \sum_{k=1}^{m} \|X_1^T(A_{k,1:m})^T - (X_{2\ k,1:(n-1)})^T\|_2^2 \tag{2.28}$$

https://doi.org/10.1017/S0956792525100247 Published online by Cambridge University Press

Let Vec(M) denote the vector obtained of stacking the successive columns of a matrix M on top of one another. Then, we can write (2.28) as:

$$\|X_1^T A^T - X_2^T\|_F^2 = \|(I \otimes X_1^T)\mathrm{Vec}(A^T) - \mathrm{Vec}(X_2^T)\|_2^2, \tag{2.29}$$

where I is the identity matrix of appropriate dimension, $\otimes$ denotes the Kronecker product. Note that (2.29) is a matrix-vector system. The problem (2.22) is therefore equivalent to the following matrix-vector NNLS problem:

$$\underset{\mathrm{Vec}(A^T)}{\arg\min} \|(I \otimes X_1^T)\mathrm{Vec}(A^T) - \mathrm{Vec}(X_2^T)\|_2, \quad \mathrm{Vec}(A^T)_j \geq 0 \ \forall j. \tag{2.30}$$

Standard NNLS algorithms (see e.g. [52]) can be applied on (2.30). Converting Vec(A^T) back into matrix form and transposing, one obtains a solution to (2.22). For small problems, this approach is feasible, and it was used throughout the present.

However, for high-dimensional data, or for datasets with many observations, the direct vectorisation approach may be untenable, due to the size of the resulting system, as the curse of dimensionality guarantees that a linear increase in the number of observations leads to quadratic increases in system size. In [58], the authors discuss several methods for solving matrix-matrix NNLS problems, including techniques that are strictly equivalent to (2.30), as well as techniques that seek sparse solutions to (2.26) directly. Note that the vectorised problem (2.30) has the structure:

$$\underset{A}{\arg\min} \left\| \begin{pmatrix} X_1^T & 0 & \dots & 0 \\ 0 & X_1^T & \dots & 0 \\ \vdots & \vdots & \ddots & \vdots \\ 0 & 0 & \dots & X_1^T \end{pmatrix} \begin{pmatrix} A_{(1,:)} \\ A_{(2,:)} \\ \vdots \\ A_{(m,:)} \end{pmatrix} - \begin{pmatrix} X_{2\,(1,:)} \\ X_{2\,(2,:)} \\ \vdots \\ X_{2\,(m,:)} \end{pmatrix} \right\|_2^2, \tag{2.31}$$

and hence can be regarded m independent NNLS problems:

$$\underset{A_{(k,:)}}{\arg\min} \|X_1^T A_{(k,:)} - X_{2\,(k,:)}\|_2^2, \ A_{(k,j)} \geq 0 \ \forall j. \tag{2.32}$$

Since X_1, X_2 are known, and each $A_{(k,:)}$ can be computed independently, (2.30) is easily parallelised. We remark that while the problems (2.30) and (2.32) are equivalent in theory, in practice, solutions to NNLS for underdetermined systems are not unique in general, and must be obtained through iterative procedures. The solutions obtained when solving the formulations (2.30) and (2.32) will, therefore, differ in practice. In the present, the authors observed that such differences were trivial; however, a comprehensive investigation of this issue was not pursued.

We remark that related work on a nonnegative DMD variant was pursued in [71]. The formulation introduced in the present differs from [71] in that we require that the approximated *operator A* be strictly nonnegative, whereas the approach in [71] requires only that the *dynamic modes*, or DMD eigenvectors, are nonnegative. However, as nonnegativity is not required for the corresponding DMD eigenvalues, the reconstructed DMD operator is not nonnegative in general. We note that this difference in formulation reflects the primary intended usage of each algorithm, as the approach in [71] was developed principally for diagnostic purposes and dimension reduction, whereas the present algorithm is intended for usage in forecasting and extrapolation.

2.3.3. Application to PWDH age structure model

We use the time- and age-dependent mortality curves obtained with the EKI for the years 2009 – 22 to forecast the evolution of the PWDH population over the years 2023 – 30. For the years 2009 – 22, we solve the model (2.1), directly applying the $\mu(a, t)$ obtained through the EKI procedure.

https://doi.org/10.1017/S0956792525100247 Published online by Cambridge University Press

To obtain mortality rates for the years 2023 – 30, we apply the nonnegative DMD algorithm outlined in section 2.3.2 defined as:

$$M = \arg\min_{M} \|M[\boldsymbol{\mu}_{2009}\ \boldsymbol{\mu}_{2010}\ \ldots\ \boldsymbol{\mu}_{2018}] - [\boldsymbol{\mu}_{2010}\ \boldsymbol{\mu}_{2011}\ \ldots\ \boldsymbol{\mu}_{2019}]\|_F,\ \ M \geq 0, \tag{2.33}$$

where the notation $M \geq 0$ indicates that M is entry-wise nonnegative. The 2023 mortality rate is then defined as $M\boldsymbol{\mu}_{2022}$, with the following years obtained by iterated multiplication by the M. We did not include the years 2020 – 22 in training the nonnegative DMD operator, as the jump in mortality rate due to COVID-19 likely represents a temporary jump in mortality, rather than a long-term trend, as indicated by preliminary 2023 mortality data returning to pre-COVID levels [2].

Similarly, we use nonnegative DMD to project age-structured annual new HIV diagnoses over the years 2023–30 as:

$$\boldsymbol{\Lambda} = \arg\min_{\boldsymbol{\Lambda}} \|\boldsymbol{\Lambda}[\lambda_{2009}\ \lambda_{2010}\ \ldots\ \lambda_{2018}] - [\lambda_{2010}\ \lambda_{2011}\ \ldots\ \lambda_{2019}]\|_F,\ \ \boldsymbol{\Lambda} \geq 0. \tag{2.34}$$

As with mortality rates, we disregard the years 2020 – 22 in projecting HIV diagnoses, as available evidence suggests that the large drop in HIV diagnoses observed in 2020, followed by rebounds in 2021 and 2020, was primarily caused by disruption and subsequent recovery in HIV testing and diagnosis [17, 78, 79]. However, estimated underlying HIV incidence continued to follow the decreasing trends observed in the years immediately preceding the COVID-19 pandemic [25]. Therefore, the increases in HIV diagnoses observed in 2021 and 2022 likely reflect a recovery of diagnoses missed during 2020 due to reduced testing, rather than changes in HIV transmission. Hence, the pre-2019 trends in new HIV diagnoses are likely more reliable for informing future trends in new HIV diagnoses over the coming years.

2.3.4. Mathematical analysis

We provide a series of results that establish the key properties of nonnegative DMD. Although the results are presented in some generality, we assume some additional conditions on the underlying data, motivated by the specific problem studied in the present. Accordingly, they may not apply universally.

Letting $X_1,\ X_2 \in \mathbb{R}^{m\times n-1}$ be as in (2.11), we assume additionally:

- *Strict positivity:*

$$(X_1)_{i,j} > 0,\ (X_2)_{i,j} > 0\ \forall\, i,\, j \tag{2.35}$$

- *Temporal regularity:*

$$(X_1)_{i,j} < 2(X_2)_{i,j},\ \ (X_2)_{i,j} < 2(X_1)_{i,j}. \tag{2.36}$$

Both assumptions hold for the data $\boldsymbol{\mu}_{2009-19},\ \lambda_{2009-19}$ used for (2.33), (2.34), respectively. The meaning of (2.35) is straightforward, and a similar assumption was employed in Theorem 1 in Section 2.1.1. Assumption (2.36) states that the local temporal variation at each observation point (age in the present document) must remain bounded, and should not more than double, or less than halve, from time-step to time-step (the factor of two is chosen for convenience). As DMD assumes underlying continuity in time [48, 67], (2.36) should hold for any data sufficiently well-resolved in time; in the absence of noise, it should be possible in principle, to obtain a time series satisfying (2.36) by increasing time-resolution of the measurements. However, we recognise that, in practice, time-series data is subject to limitations and (2.36) may not hold in general.

Theorem 2. *Any M solving (2.33), or $\boldsymbol{\Lambda}$ solving (2.34), is nonzero.*

Proof. *We provide a result for Problem (2.33), and note that an identical argument applies to (2.34). We prove contrapositive of the theorem statement, and show that if M is a matrix containing only zeroes,*

https://doi.org/10.1017/S0956792525100247 Published online by Cambridge University Press

it cannot be a solution of (2.33). For ease of notation, let:

$$\widehat{\boldsymbol{\mu}}_{2009-18} = [\boldsymbol{\mu}_{2009}\ \boldsymbol{\mu}_{2010}\ \dots\ \boldsymbol{\mu}_{2018}], \qquad \widehat{\boldsymbol{\mu}}_{2010-19} = [\boldsymbol{\mu}_{2010}\ \boldsymbol{\mu}_{2011}\ \dots\ \boldsymbol{\mu}_{2019}], \tag{2.37}$$

and proceed by contradiction. Denote as $\vec{0} \in \mathbb{R}^{m\times m}$ *the* $m \times m$ *matrix whose entries are identically zero, and suppose that* $\vec{0}$ *solves (2.33). Then:*

$$\|\vec{0}\widehat{\boldsymbol{\mu}}_{2009-18} - \widehat{\boldsymbol{\mu}}_{2010-19}\|_F = \|\widehat{\boldsymbol{\mu}}_{2010-19}\|_F \leq \|A\widehat{\boldsymbol{\mu}}_{2009-18} - \widehat{\boldsymbol{\mu}}_{2010-19}\|_F\ \forall A \geq 0. \tag{2.38}$$

Let I *be the* $m \times m$ *identity matrix. Clearly* $I \geq 0$*. Observe that:*

$$\|I\widehat{\boldsymbol{\mu}}_{2009-18} - \widehat{\boldsymbol{\mu}}_{2010-19}\|_F = \|\widehat{\boldsymbol{\mu}}_{2009-18} - \widehat{\boldsymbol{\mu}}_{2010-19}\|_F. \tag{2.39}$$

Squaring the right-hand side of (2.39) and applying the definition of the Frobenius norm gives:

$$\begin{aligned}
\sum_{j=2009}^{2018} \|\boldsymbol{\mu}_j - \boldsymbol{\mu}_{j+1}\|_2^2 &= \sum_{j=2009}^{2018}\sum_{i=1}^{m} (\mu_{i,j} - \mu_{i,j+1})^2 \\
&= \sum_{j=2009}^{2018}\sum_{i=1}^{m} \mu_{i,j}^2 + \mu_{i,j+1}^2 - 2\mu_{i,j}\mu_{i,j+1} \\
&< \sum_{j=2009}^{2018}\sum_{i=1}^{m} 2\mu_{i,j}\mu_{i,j+1} + \mu_{i,j+1}^2 - 2\mu_{i,j}\mu_{i,j+1} \\
&= \sum_{j=2009}^{2018}\sum_{i=1}^{m} \mu_{i,j+1}^2 \\
&= \|\widehat{\boldsymbol{\mu}}_{2010-19}\|_F^2,
\end{aligned} \tag{2.40}$$

where the third line follows from the temporal regularity assumption (2.36). From (2.40), it follows that:

$$\|I\boldsymbol{\mu}_{2009-18} - \boldsymbol{\mu}_{2010-19}\|_F < \|\boldsymbol{\mu}_{2010-19}\|_F = \|\vec{0}\,\boldsymbol{\mu}_{2009-18} - \boldsymbol{\mu}_{2010-19}\|_F, \tag{2.41}$$

contradicting (2.38), implying that the zero matrix cannot be a solution of (2.34), as was to be shown. □

Interpretation in terms of the Perron-Frobenius operator. In this portion of the article, we provide an interpretation of nonnegative DMD in terms of the Perron-Frobenius (P-F) operator. We note that numerical methods for the P-F operator have been studied in other settings [9, 18, 44, 46]. DMD is generally interpreted as a numerical approximation of the *Koopman operator*, the adjoint of the P-F operator [12, 48]. Roughly speaking, the Koopman operator acts on functions of the system state (commonly called *observables*), while the P-F operator acts on *densities* of the system state.

Since the P-F and Koopman operators are adjoint, one can use either to describe a given dynamical system [51]. Nonetheless, the literature on the numerical approximation of the two operators is somewhat distinct. Literature on the approximation of the P-F operator tends to focus on *Ulam's method* and its variants [9, 18, 19, 21, 38, 44], while the approximation of the Koopman operator focuses on DMD and its variants [4, 12, 15, 48, 62]. Note that this statement is only a broad, general characterisation, and several works discuss the approximation of both operators [43–45] and/or hybrid-type approaches incorporating aspects of both DMD and Ulam's method [14, 29].

In the following, we describe why, in the context of the present work, and problem (2.33) in particular, the P-F operator provides a natural interpretation. We remark that a full description of the P-F and Koopman operators is beyond the scope of the current work, and we recommend that the reader consult [43] for a comprehensive discussion of the numerical approximation of the P-F and Koopman operators, and [51] for the underlying theory. We note that this description is not, nor is intended to be, fully rigorous. Rather, it is intended as an intuitive explanation for the nonnegative DMD formulation used

https://doi.org/10.1017/S0956792525100247 Published online by Cambridge University Press

herein, and how it differs from other common DMD approaches within the context of Koopman/P-F theory.

Consider a measure space defined by the three-tuple $\mathcal{M} := (\mathbb{A}, \mathfrak{B}, \nu)$ where $\mathbb{A} = \mathbb{R}^+ = [0, \infty)$, the nonnegative real numbers, is the space of possible ages, $\mathfrak{B}$ is a $\sigma-$algebra on $\mathbb{A}$ and ν the Lebesgue measure. Let $S{:}\mathbb{A} \to \mathbb{A}$ be a measurable mapping which advances the age of the population. For simplicity and without the loss of generality, we assume S advances age forward one unit; hence, S moves a member of the population aged a to age $a + 1$. For simplicity, we disregard new entries $\lambda(a, t)$ for the moment.

Let $u_t(a) \in \mathcal{L}^1(\mathbb{A},\ \nu)$ describe the population distribution at time t, with an initial datum $u_0 \in \mathcal{L}(\mathbb{A},\ \nu)$ assumed known. We define the *support* of u_t as:

$$\text{supp}(u_t) := \{a \in \mathbb{A} | u_t(a) \neq 0\}. \tag{2.42}$$

Since human lifespans are finite, we may assume:

$$\nu(\text{supp}(u_t)) < \infty. \tag{2.43}$$

at all t.

Since $u_t(a) \in \mathcal{L}^1(\mathbb{A},\ \nu),\ u_t(a) \geq 0\ \forall\ a \in \mathbb{A}$, we may also define the *population measure* $\widehat{u}_t \in \mathcal{M}$:

$$\widehat{u}_t(X) = \int_X u_t(a)da, \quad X \in \mathfrak{B}. \tag{2.44}$$

Define the three-tuple $\widehat{\mathcal{M}} := (\mathbb{A},\ \mathfrak{B},\ \widehat{u}_t)$ and let $\widehat{\mu}_t(X) \in \widehat{\mathcal{M}}$ be the *mortality measure* at a time t, measuring the number of deaths in the age-set X of the population u at time t. Clearly, if $\widehat{u}_t(X) = 0$ for some $X \in \mathfrak{B}$, then $\widehat{\mu}_t(X) = 0$ and hence, by the Radon-Nikodym theorem [51], there exists a density function $\mu_t \in \mathcal{L}^1(\mathbb{A},\ \widehat{u}_t)$ such that:

$$\widehat{\mu}_t(X) = \int_X \mu_t(a)\widehat{u}_t(da) = \int_X \mu_t(a)u_t(a)da, \quad X \in \mathfrak{B}. \tag{2.45}$$

We note that the algorithm 1 reconstructs discrete represenations $\boldsymbol{\mu}_t$ of the *density* $\mu_t(a)$ above, and not of the measure $\widehat{\mu}_t$. From the Riesz Representation Theorem [51], there is a linear operator $\psi_t(u)$ on the dual space of $\mathcal{L}^1(\mathbb{A}, \nu)$ such that for any $u \in \mathcal{L}^1(\mathbb{A}, \nu)$:

$$\psi_t(u) := \int_0^\infty u(a)\widehat{\mu}_t(da) = \int_0^\infty u(a)\mu_t(a)da = (u,\ \mu_t) = \widehat{\mu}_t(\mathbb{A}), \tag{2.46}$$

where $(\cdot,\ \cdot)$ indicates the scalar product.

We now recall that our nonnegative DMD operator A is recovered as the solution of:

$$\arg\min_{A^T} \|X_1^T A^T - X_2^T\|_F, \quad A_{i,j}^T \geq 0\ \forall i,\ j. \tag{2.47}$$

For the sake of concreteness, suppose we are considering the mortality rate-recovery problem (2.33). Then, the matrices X_1 and X_2 have the structures:

$$X_1^T = \begin{pmatrix} \boldsymbol{\mu}_{2009}^T \\ \boldsymbol{\mu}_{2010}^T \\ \vdots \\ \boldsymbol{\mu}_{2018}^T \end{pmatrix}, \qquad X_2^T = \begin{pmatrix} \boldsymbol{\mu}_{2010}^T \\ \boldsymbol{\mu}_{2011}^T \\ \vdots \\ \boldsymbol{\mu}_{2019}^T \end{pmatrix}. \tag{2.48}$$

Heuristically, we may regard the discrete expression $\boldsymbol{\mu}_t^T u$ as an analogue of:

$$\boldsymbol{\mu}_t^T u \approx \int_0^\infty u(a)\widehat{\mu}_t(da) = (u,\ \mu_t) = \psi_t(u). \tag{2.49}$$

Following a similar intuition as used in (2.49), we note that the expression:

$$(AX_1)^T u = X_2^T u \tag{2.50}$$

https://doi.org/10.1017/S0956792525100247 Published online by Cambridge University Press

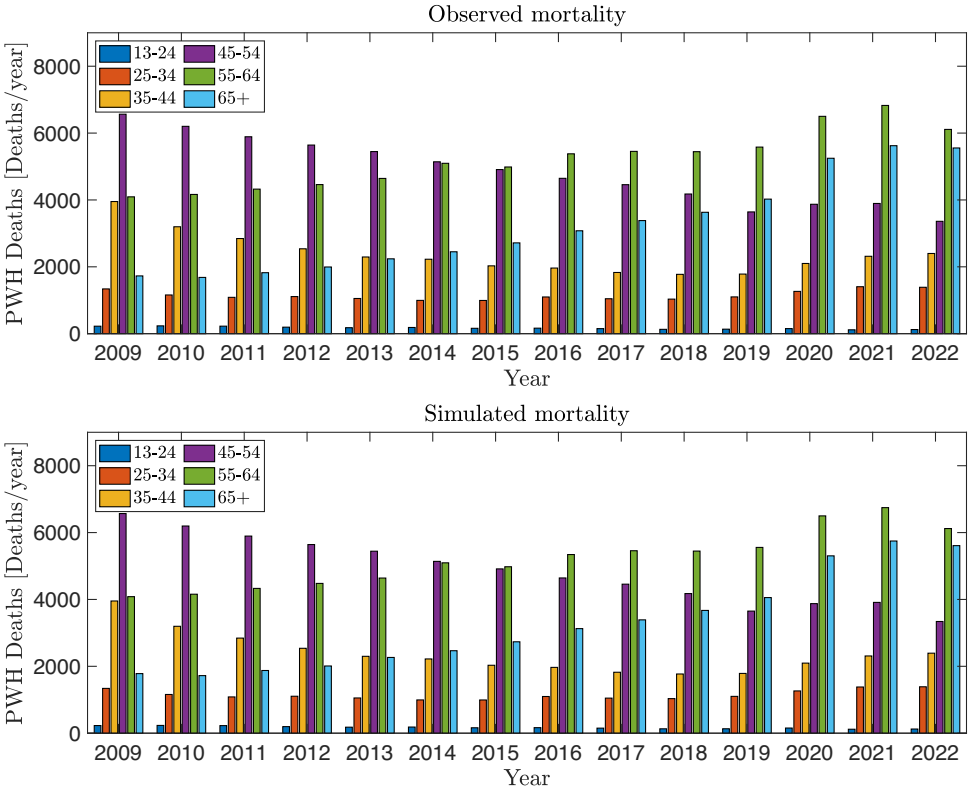

Figure 2. *The comparison of surveillance (top) and simulated (bottom) mortality.*

is a discrete analogue of:

$$(u,\ A\mu_t) = (u,\ \mu_{t+1}) \tag{2.51}$$

which, together with (2.46):

$$\psi_{t+1}(u) = (u, \mu_{t+1}) = (u, A\mu_t) = (A^*u, \mu_t) = \psi_t(A^*u) = A\psi_t(u). \tag{2.52}$$

Consequently, the nonnegative DMD operator can be interpreted as an approximation of the *Perron-Frobenius operator* applied to the mortality measures $\widehat{\mu}_t$ (or their related densities concerning the population measure), thereby evolving them over time [51]. By employing NNLS to compute A, we ensure that the projected μ_t remain on the positive cone and in $\mathcal{L}^1(\mathbb{A}, \widehat{u}_t)$ for every t. In other words, nonnegative DMD guarantees that densities are transformed into densities, as desired.

3. Results

3.1. Reconstruction of age-dependent PWDH mortality curves, 2009 – 22

By applying the Kalman Inversion procedure outlined in the previous section, we observe a strong agreement with the data in Figure 2. This figure illustrates the age distribution of mortality for each year, juxtaposing real data (top panel) with simulated mortality (bottom panel). The simulated and observed mortality are in agreement both qualitatively and quantitatively. We provide the full numerical comparison against surveillance data, each year and age bracket, in Table A1 in an appendix at the end of the main text.

https://doi.org/10.1017/S0956792525100247 Published online by Cambridge University Press

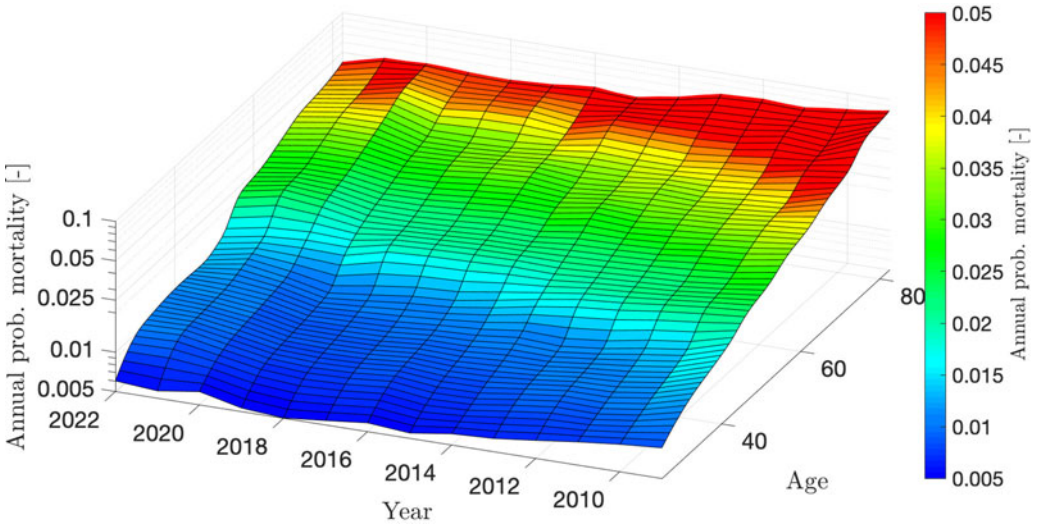

Figure 3. *Annual probability of mortality at a given age, in time. Note the consistent decrease in time, punctuated by increases in the upper age ranges in 2020–22 caused by the COVID-19 pandemic.*

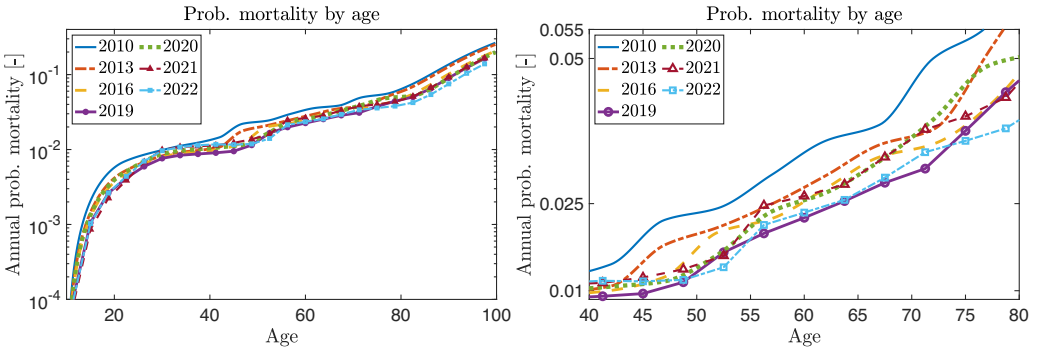

Figure 4. *Mortality curves by age for several years, plotted side-by-side. The left panel shows mortality probability over the entire age range; the right panel focuses more closely on the important 40–80 age range.*

In Figure 3, we depict the annual mortality rate per age class over time. The colour scale ranges from 0.005 (dark blue) to 0.04 (red). This visualisation indicates a trend of decreasing annual mortality, evidenced by the expanding blue regions from 2010 to 2022. However, we note that at the beginning of the COVID-19 pandemic (2020), this trend slows somewhat, and mortality rates increases slightly. The red and yellow regions, which correspond to mortality rates at older ages, also show a strong diminishing trend in time until the beginning of the COVID-19 pandemic. The results suggest that the COVID-19 pandemic caused mortality rates across the 55 + age cohorts over the years 2020–21 to revert approximately to their approximate 2013 levels [26, 77].

In Figure 4, we depict several age-dependent mortality curves for individual years, over the entire age range (left panel), and focusing on the important 40 – 80 age range (right panel). Mortality decreases throughout the entire age range; however, as noted previously, these trends reverse in 2020, and mortality rates over the years 2020–21 increase among the 55 + cohort to levels similar to 2013–16. The 2022 rates show the effects of COVID subsiding among the 55 + cohort, with mortality rates consistent with levels observed during the years 2016 – 19 among PWDH aged 55–75, and at their lowest rates ever for PWDH aged 75 +. However, we note that, even during the peak years of COVID-19 in 2020–21,

https://doi.org/10.1017/S0956792525100247 Published online by Cambridge University Press

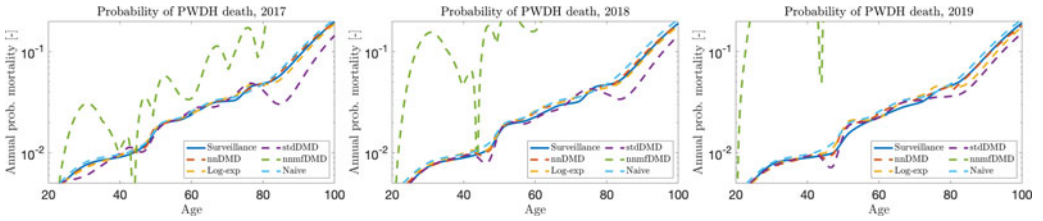

Figure 5. *Comparison of data-driven forecasts against surveillance reconstructions, 2017–19 (left--to-right). We observe that nonnegative DMD provides the most consistently accurate, and stable reconstructions.*

mortality among older PWDH was still lower than 2010 levels, which suggests that the effects driving the decreases in mortality risk among PWDH over the past 15 years were more significant, on net, than the effects of the COVID-19 pandemic on PWDH mortality.

3.2. Nonnegative DMD forecasting validation

In this subsection, we provide a brief study comparing the suitability of nonnegative DMD in forecasting the evolution of age-dependent PWDH mortality.

3.2.1. Test setup

We consider the reconstructed age-dependent mortality rates used in the main text. We use the reconstructed years 2009–16 as training data, and then compare the forecasts with the reconstructed data over the window 2017–19. We compare the following forecasting algorithms:

(1) *Standard DMD*, defined as (2.13) in the main text;

(2) *Nonnegative matrix factorisation DMD*, defined as (2.15) in the main text;

(3) *Nonnegative DMD*, defined as (2.22) in the main text;

(4) *Log-exp DMD*, defined as (2.16), (2.17) in the main text;

(5) *Naive approach*, which simply uses the reconstructed age-dependent mortality for the year 2016 for each subsequent year 2017 – 19.

We evaluate each forecasting method by comparing the relative L^2 error of the forecasted mortality curve $\boldsymbol{\mu}_j^F$ to the reconstructed curve $\boldsymbol{\mu}_j$ for each year $j = 2017, 2018, 2019$.

3.2.2. Numerical results

In figure 5, we plot the forecasts for each method, for each year, over the period 2017 – 19. As expected, the NNMF DMD (2.15) produces noisy, nonphysical extrapolations. Standard DMD (2.13) shows oscillatory behaviour and poor accuracy. The log-exp DMD approach (2.16) provides more accurate forecasts than standard or NNMF DMD; however, by 2019, oscillations appear, degrading forecasting accuracy. In contrast, nonnegative DMD (2.22) produces stable forecasts over the entire time period. In Table 1, we report the relative L^2 error for each forecasting method, for each year, which confirm that nonnegative DMD provides more accurate forecasts.

In Figure 6, we show the 10-year forecast for different DMD variants, as well as the naive approach. While data are not available to evaluate accuracy, we observe that the nonnegative DMD (2.22) is notably more *plausible* compared to the alternative approaches. Both standard DMD (2.13) and the log-exp DMD (2.16) exhibit nonphysical, implausible oscillations. The NNMF-based approach (2.15)

https://doi.org/10.1017/S0956792525100247 Published online by Cambridge University Press

Table 1. *Comparison of L^2 error for age-dependent mortality rates for different algorithms (trained through 2016; forecast 2017 – 19)*

Year	Std. DMD	NNMF DMD	Nonneg. DMD	Log-exp DMD	Naive
2017	0.344	5.21	0.039	0.066	0.088
2018	0.287	25.18	0.034	0.058	0.131
2019	0.229	94.87	0.044	0.123	0.106

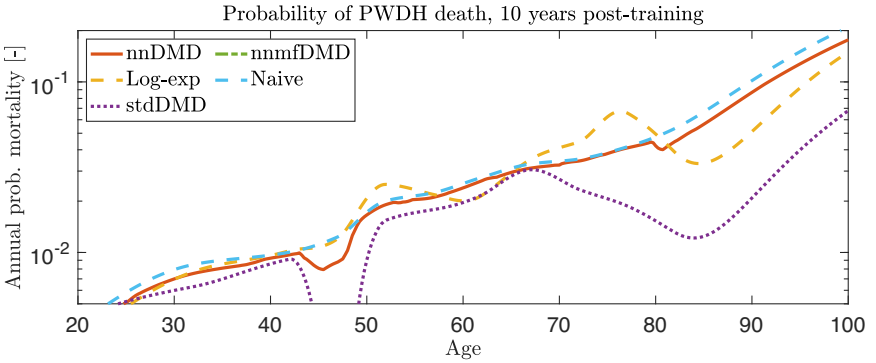

Figure 6. *Comparison of the different mortality forecasting approaches over a 10-year time horizon. We observe that nonnegative DMD produces less oscillatory forecasts when projected over longer timeframes. In contrast, standard DMD and log-exp approaches are prone to nonphysical oscillation.*

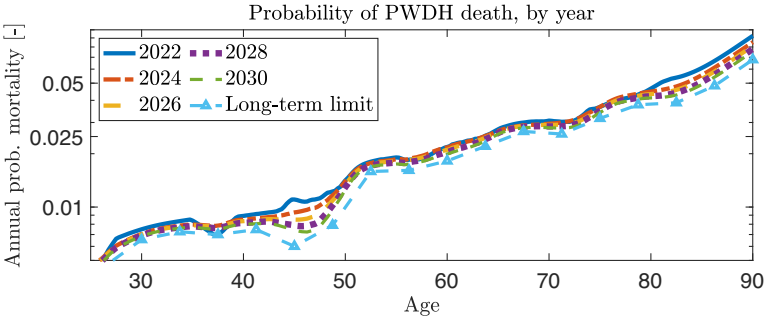

Figure 7. *Projection of age-dependent mortality through 2030. The maximum eigenvector is the asymptotic limit of the projected future age-dependent PWDH mortality.*

is no longer visible due to the oscillations and blowup. Hence, we confirm that nonnegative DMD (2.22), in addition to being more accurate over short time horizons, is also robust over longer time horizons.

3.3. Forecasting PWDH mortality, new diagnoses and PWDH population age-structure, 2023-30

3.3.1. Future PWDH mortality

In order to forecast the evolution of the mortality rate per age-class, we employ the nonnegative DMD as described in Section 2.3.3. In Figure 7, we depict the annual age-dependent probability of mortality for the years 2022, 2024, 2026, 2028 and 2030. The nonnegative DMD algorithm forecasts mortality rates to continue decreasing substantially in the 40 – 55 age range, with annual mortality projected to decrease 15.6% in this age group from 2022 to 2030. Among PWDH aged 55 – 75, we also project future decreases in mortality, however, these are comparatively modest, decreasing approximately 7.5%

https://doi.org/10.1017/S0956792525100247 Published online by Cambridge University Press

from 2022 to 2030. For PWDH aged 75 to 90, mortality is projected to decrease approximately 15.6% from 2022 to 2030.

Analysing the spectrum of M, we find that it has a unique maximum eigenvalue $\xi_1 = \rho(M) = 1$ (consistent with the interpretation of M as an approximation of the P-F operator [43, 51]), with second-largest eigenvalue $|\xi_2| = 0.87$. We denote the corresponding eigenvectors as v_1 and v_2, respectively, and express $\boldsymbol{\mu}_{2022}$ as a linear combination of the eigenvectors v_i of M:

$$\boldsymbol{\mu}_{2022} = \sum_i a_i v_i. \tag{3.1}$$

Observe that:

$$\lim_{k\to\infty} M^k \boldsymbol{\mu}_{2022} = 1^k a_1 v_1 + 0.87^k a_2 v_2 + \sum_{i\geq 3} \xi_i^k a_i v_i = a_1 v_1, \tag{3.2}$$

since $|\xi_i| \leq .8909 < 1,\ \forall i \geq 3$.

The eigenvector $a_1 v_1$ of M corresponding to $\xi_1 = 1$ thus gives a long-term projection for the asymptotic age-dependent PWDH mortality rate, with age-dependent PWDH mortality converging to $a_1 v_1$ like $.87^t$. We plot this eigenvector as 'Max eigenvector' in Figure 7. As the figure shows, beyond 2030, mortality among PWDH is projected to decrease significantly among PWDH aged 35 – 55 older than 80, and moderately among PWDH aged 60 – 80. We note that these forecasts are based on pre-2019 trends in PWDH mortality and hence cannot account for any changes beyond those pre-existing trends. As such, these forecasts, especially the asymptotic limit, should be interpreted with caution.

Remark. As M is nonnegative, if it is additionally irreducible, then we can guarantee that v_1 has strictly positive entries from the Perron-Frobenius theorem. However, establishing irreducibility for a general M is difficult, given the lack of a closed-form expression. Nonetheless, our experiments over an ensemble of M consistently showed that M has a unique maximum eigenvalue of 1, with a strictly positive corresponding eigenvector (we note that the spectral gap varied across the different M).

3.3.2. Future HIV diagnoses

To forecast future new HIV diagnoses by age, we employed the nonnegative DMD algorithm on the age-depdendent diagnosis data as in (2.34). These data were defined using NCHHSTP surveillance data [26]. New HIV diagnoses are projected to decrease at approximately 3% per year, declining to approximately 28,000 new diagnoses in 2030. Furthermore, the age structure of new HIV diagnoses is not projected to show significant change in the coming years. We depict both the number and percentage of new HIV diagnoses by age group in Figure 8.

3.3.3. PWDH population age structure, 2023–30

Using projected PWDH mortality (2.33) and projected new HIV diagnoses (2.34), we solve the system (2.1) through year-end 2030 to project the evolution of the PWDH age-structure over the years 2023-30.

The total PWDH population is projected to grow over the simulation period, increasing to 1,160,000 by the end of 2030. As a whole, the PWDH population is also projected to age significantly and rapidly in the coming years. At year-end 2024, an estimated 42.5% of PWDH were 55 and older, 19.4% 65 and older and 4.2% 75 and older. By year-end 2030, we project the percentage of PWDH over 55 to increase to 47.% and those over 65 to 26.1%. The percentage of PWDH over 75 is projected to more than double over a five year span, reaching 8.5%, by the end of 2030. This information is depicted in Figure 9.

We remark, however, that not all age groups are projected to increase uniformly. As discussed in the previous subsections, future PWDH mortality rates are projected to decrease, however, such decreases are vary heavily with age. Conversely, while new HIV diagnoses are expected to decrease, the projected age distribution does not show significant change. By 2030, this results in the formation of a bimodal-like

https://doi.org/10.1017/S0956792525100247 Published online by Cambridge University Press

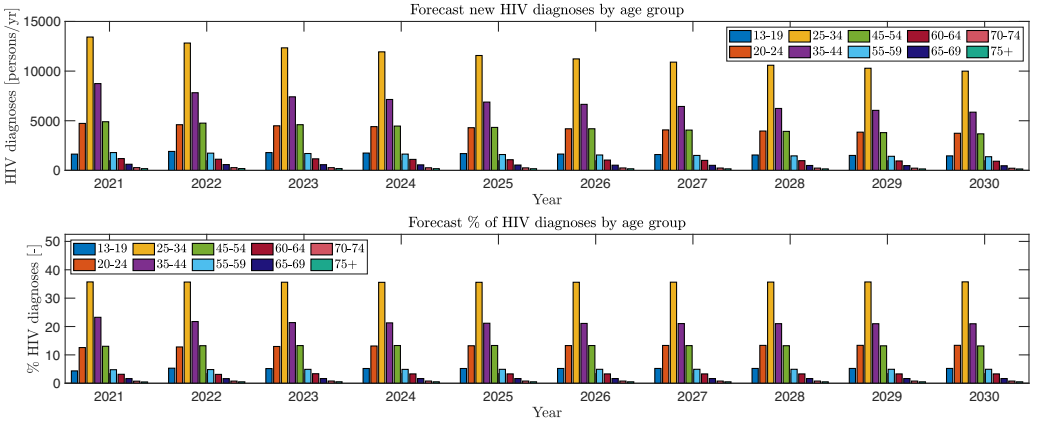

Figure 8. *Projection of age-dependent HIV diagnoses through 2030. We project a slight decrease in overall diagnoses, with approximately 28,000 new HIV diagnoses in 2030 (compared to 34,500 in 2023).*

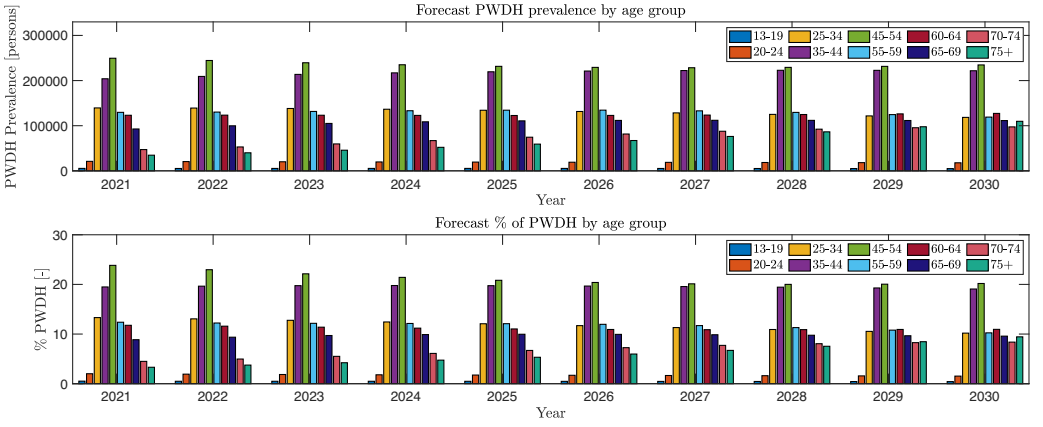

Figure 9. *Projection of the PWDH age structure in the United States through 2030. We observe a gradual ageing of the PWDH population. By 2030, 48.6% of the PWDH population is projected to be over 55 and 27.4% over 65.*

population PWDH age distribtution, in which there are fewer PWDH approximately aged 50 compared to either age 40 and age 60 (Figure 10).

4. Discussion

In the present work, we have examined age-dependent data on PWDH in the United States to better understand how the developments over the previous 15 years have changed the age structure of the PWDH population in the United States and, furthermore, what implications these changes may have going forward. Starting with a simple age-structured population model, we used an EnKF Inversion, together with discrete age-structured HIV surveillance data, to reconstruct age-dependent PWDH mortality over the years 2008–22. We found that, due to the widespread availability of effective ART, mortality has declined significantly among PWDH since 2008, particularly among PWDH aged 40–80 years. While this trend reversed somewhat among PWDH aged 55 and older in 2021–22 due to the COVID-19 pandemic, data from 2022 suggest that COVID effects have subsided, likely signalling a return to pre-COVID trends.

https://doi.org/10.1017/S0956792525100247 Published online by Cambridge University Press

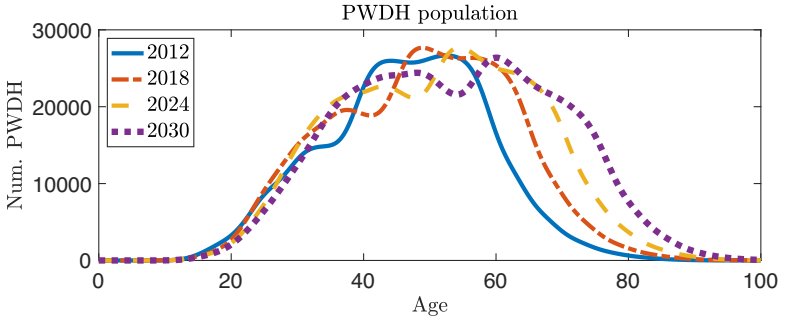

Figure 10. *Evolution of the PWDH population age structure over the years 2012–2030. By year-end 2030, we see a bimodal distribution forming, with more PWDH around age 40 and age 60, as compared to PWDH around age 50.*

We then developed a novel variant of DMD, nonnegative DMD, to develop projections of future changes in PWDH mortality and diagnoses. Projections of future PWDH mortality rates suggest that PWDH mortality will continue to decrease in the coming years, with the largest decreases expected among PWDH aged 40–55 and those older than 80. While mortality rates are expected to decrease among other age groups as well, smaller decreases are projected. We note that these projections assume a continuation of pre-existing trends, and cannot account for major changes in the coming years, such as medical breakthroughs.

Our projections of future HIV diagnoses suggest a slow, but notable, decrease in annual HIV diagnoses going forward, with around 28,000 diagnoses projected in 2030. Interestingly, our methods did not indicate a major change in the age structure of new HIV diagnoses, which has remained largely static in recent years, and is projected to remain so.

Applying our reconstructed and projected mortality and diagnosis data to our core PWDH age model, we then projected the age structure of the PWDH population over the coming years. Our simulations suggest that the PWDH population will age significantly. By 2030, the percentage of PWDH aged 55 years and older is expected to increase significantly (from 40% to 47.4%). Furthermore, these increases are more dramatic for older age groups; the percentage of PWDH aged 65 and older is expected to increase to 26.1% by 2030, and the portion of those aged 75 years and older is expected to more than double by 2030.

We note that the analysis is subject to several important limitations. As previously mentioned, the projections of future changes in PWDH mortality and diagnoses assume continuation of pre-existing trends. It is possible that new medical technologies may alter the landscape of HIV prevention and care significantly. This is particularly important for new HIV diagnoses, as improvements such as rapid expansion of pre-exposure prophylaxis (PrEP) coverage or increased levels of viral suppression (e.g. due to long-acting injectable ART [76]), may result in fewer new HIV diagnoses than projected [20]. Furthermore, new HIV diagnoses were modelled as a linear source term, and any dependence on the PWDH age structure is assumed to be captured implicitly via any trends present in the data. However, the relationship between new the quantity and age distribution of new HIV diagnoses and the current PWDH population state may be more complex, and future modelling efforts should seek to better explore and define this relationship.

Crucially, the current analysis represents only a first step towards developing comprehensive models for ageing in the PWDH population. Future extensions should include other aspects of HIV prevention and care. For example, beyond biological age, time since acquiring HIV infection and time on ART may also be important factors in determining risk for certain comorbidities. Other extensions, including demographic stratification, may be similarly significant.

The techniques used for data-driven mortality forecasting used herein, while effective capturing the relevant dynamics, are not particularly interpretable, limiting their usefulness outside of forecasting.

https://doi.org/10.1017/S0956792525100247 Published online by Cambridge University Press

In reality, distinct processes underlie these dynamics: ART uptake/adherence, stigma/social determinants of health, as well as all the same trends driving increased longevity in the general population. Techniques such as those shown in [36] may potentially be used to identify and distinguish the different processes underlying these dynamics. Such information is crucial for model-informed intervention planning.

On the mathematical end, further analysis of nonnegative DMD is necessary. In the present work, we introduced the basics of the method and provided some elementary results for the current problem, as well as some intuitive arguments. Given the application-oriented nature of the current work, we elected to leave further exploration to future research. However, it is important to properly formalise how nonnegative DMD fits within the larger family of DMD methods. More rigorous analysis is necessary to establish when certain conditions observed in the current analysis, such as the existence of a limiting eigenvector with an associated simple eigenvalue of 1, can be expected to hold. Finally, developing more sophisticated and efficient computational approaches for nonnegative DMD, particularly those that exploit its parallelizability, are important for extending its application to larger-scale problems.

Our analysis highlights the urgent need to prepare for the ageing population of PWDH. Current data suggest that PWDH are more vulnerable to ageing-related comorbidities, requiring that the healthcare system be properly equipped to handle the potential rapid increase in such health conditions. Furthermore, in the case of preventable age-related comorbidities, the current analysis also emphasises the need to develop and implement prevention programmes to help reduce potential burden on the healthcare system as much as possible. Urgency is necessary, as model projections show that the portion of PWDH aged 75 and older will more than double over a five-year span. Beyond HIV care, using mathematical models to account for ageing populations is an important direction for research in public health, and its importance is likely to increase in importance in the coming years.

Acknowledgments. The authors would like to acknowledge Stefan Klus, Matthew Colbrook, Nicolas Nadisic, Siobhan O'Connor, Paul G. Farnham, Dr. John Brooks, and Ruiguang Song for their helpful input and advice. The authors are the members of the INDAM GNCS (Italian National Group of Scientific Calculus).

Funding statement. E. Iacomini is partially supported by the Italian Research Center on High-Performance Computing, Big Data and Quantum Computing (ICSC) funded by MUR Missione 4-Next Generation EU (NGEU) [Spoke 1 'Future HPC & Big Data'].

Competing interest. The authors declare none.

References

[1] Aanonsen, S. I., Naevdal, G., Oliver, D. S., Reynolds, A. C. & Valles, B. (2009) The ensemble Kalman filter in reservoir engineering–a review. *SPE J* **3**, 393–412.

[2] Ahmad, F. B., Cisewski, J. A. & Anderson, R. N. (2024) Mortality in the United States—provisional data, 2023. *MMWR Morb. and Mortal. Wkly Rep*. **73**, 677–681.

[3] Alla, A., Balzotti, C., Briani, M. & Cristiani, E. (2020) Understanding mass transfer directions via data-driven models with application to mobile phone data. *SIAM J. Appl. Dyn. Syst.* **19** (2), 1372–1391.

[4] Alla, A., Monti, A. & Sgura, I. (2024) Piecewise DMD for oscillatory and Turing spatio-temporal dynamics. *Comput. Math. Appl.* **160**, 108–124.

[5] Althoff, K. N., Stewart, C., Humes, E., *et al.* (2024) The forecasted prevalence of comorbidities and multimorbidity in people with HIV in the United States through the year 2030: A modeling study. *Plos Med.* **21** (1), e1004325.

[6] Barros, G. F., Grave, M., Viguerie, A., Reali, A. & Coutinho, A. L. (2021) Dynamic mode decomposition in adaptive mesh refinement and coarsening simulations. *Eng. Comput.* **38** (5), 4241–4268.

[7] Bigna, J. J., Ndoadoumgue, A. L., Nansseu, J. R., *et al.* (2020) Global burden of hypertension among people living with HIV in the era of increased life expectancy: A systematic review and meta-analysis. *J. Hypertens.* **38** (9), 1659–1668.

[8] Bloch, M., John, M., Smith, D., Rasmussen, T. & Wright, E. (2020) Managing HIV-associated inflammation and ageing in the era of modern ART. *HIV Med.* **21**, 2–16.

[9] Bollt, E. M. & Santitissadeekorn, N. (2013) *Applied and computational measurable dynamics*. Society for Industrial and Applied Mathematics.

[10] Bosh, K. A. (2020) Vital signs: Deaths among persons with diagnosed HIV infection, United States, 2010–2018. *MMWR. Morbidity and Mortality Weekly Report* **69**.

https://doi.org/10.1017/S0956792525100247 Published online by Cambridge University Press

[11] Böttcher, L., Chou, T. & D'Orsogna, M. R. (2024) Forecasting drug-overdose mortality by age in the United States at the national and county levels. *PNAS Nexus* **3** (2), pgae050.
[12] Brunton, S. L., Budisic, M., Kaiser, E. & Kutz, J. N. (2022) Modern Koopman theory for dynamical systems. *SIAM Rev.* **64** (2), 229–340.
[13] Chawla, A., Wang, C., Patton, C., *et al.* (2018) A review of long-term toxicity of antiretroviral treatment regimens and implications for an aging population. *Infect. Dise. Ther.* **7**, 183–195.
[14] Colbrook, M. J. (2023) The mpEDMD algorithm for data-driven computations of measure-preserving dynamical systems. *SIAM J. Numer. Anal.* **61** (3), 1585–1608.
[15] Colbrook, M. J., Ayton, L. J. & Szőke, M. (2023) Residual dynamic mode decomposition: robust and verified Koopmanism. *J. Fluid Mech.* **955**, A21.
[16] Collins, L. F. & Armstrong, W. S. (2020) What it means to age with HIV infection: Years gained are not comorbidity free. *JAMA Netw. Open* **3** (6), e208023–e208023.
[17] DiNenno, E. A. (2022) *HIV testing before and during the COVID-19 pandemic—United States, 2019–2020. MMWR. Morbidity and Mortality Weekly Report* **71**(25), 820–825.
[18] Ding, J., Du, Q. & Li, T.-Y. (1993) High order approximation of the Frobenius-Perron operator. *Appl. Math. Comput.* **53** (2–3), 151–171.
[19] Ding, J. & Li, T. Y. (1991) Markov finite approximation of Frobenius-Perron operator. *Nonlinear Anal.: Theory, Methods Appl.* **17** 8), 759–772.
[20] Eisinger, R. W. & Fauci, A. S. (2018) Ending the HIV/AIDS pandemic. *Emerg. Infect. Dis.* **24** (3), 413.
[21] Ermann, L. & Shepelyansky, D. L. (2010) Ulam method and fractal Weyl law for Perron-Frobenius operators. *Eur. Phys. J. B* **75**, 299–304.
[22] Evensen, G. (1994) Sequential data assimilation with a nonlinear quasi-geostrophic model using Monte Carlo methods to forecast error statistics. *J. Geophys. Res.* **99**, 10143–10162.
[23] Evensen, G. & Van Leeuwen, P. J. (1996) Assimilation of geosat altimeter data for the agulhas current using the ensemble Kalman filter with a quasi-geostrophic model. *Mon. Weather* **128**, 85–96.
[24] Fonzi, N., Brunton, S. L. & Fasel, U. (2020) Data-driven nonlinear aeroelastic models of morphing wings for control: Data-driven nonlinear aeroelastic models. *Proc. Math. Phys. Eng. Sci.* **476** (2239), 20200079.
[25] C. for Disease Control and Prevention (2024) *Estimated HIV incidence and prevalence in the United States, 2018–2022*. HIV Surveillance Report, 29 (1).
[26] C. for Disease Control and Prevention (2024) NCHHSTP AtlasPlus. https://gis.cdc.gov/grasp/nchhstpatlas/tables.html
[27] Fosnacht, A. M. (2013). *Older Adults with HIV: An in-Depth Examination of an Emerging Population*, Vol. **127**, Hauppague, ny, Nova publishers, pp. 117.(hardback).
[28] Golub, G. H. & Van Loan, C. F. (2013) *Matrix Computations*, JHU press.
[29] Goswami, D., Thackray, E. & Paley, D. A. (2018) Constrained Ulam dynamic mode decomposition: Approximation of the Perron-Frobenius operator for deterministic and stochastic systems. *IEEE Control Syst. Lett.* **2** (4), 809–814.
[30] Guaraldi, G., Prakash, M. & Moecklinghoff, C., *et al.* (2014) *Morbidity in older HIV-infected patients: Impact of long-term antiretroviral use. AIDS Rev.* **16** (2), 75–89.
[31] Gueler, A., Moser, A., Calmy, A., *et al.* (2017) Life expectancy in HIV-positive persons in Switzerland: Matched comparison with general population. *AIDS* **31** (3), 427–436.
[32] Herty, M. & Iacomini, E. (2023) Filtering methods for coupled inverse problems. *SIAM J. Appl. Dyn. Syst.* **22** (2), 1234–1252.
[33] Herty, M., Iacomini, E. & Visconti, G. (2022) Recent trends on nonlinear filtering for inverse problems. *Commun. Appl. Ind. Math.* **13** (1), 10–20.
[34] Herty, M. & Visconti, G. (2019) Kinetic methods for inverse problems. *Kinet. Relat. Mod.* **12** (5), 1109–1130.
[35] Hyle, E. P., Kasaie, P., Schwamm, E., *et al.* (2023) A growing number of men who have sex with men aging with HIV (2021 – 2031): A comparison of two microsimulation models. *J. Infect. Dis.* **227** (3), 412–422.
[36] Ichinaga, S. M., Brunton, S. L., Aravkin, A. Y. & Kutz, J. N. (2025) Sparse-mode dynamic mode decomposition for disambiguating local and global structures. arXiv preprint arXiv: 2507.19787.
[37] Janjic, T., McLaughlin, D., Cohn, S. E. & Verlaan, M. (2014) Conservation of mass and preservation of positivity with ensemble-type Kalman filter algorithms. *Mon. Weather Rev.* **142** (2), 755–773.
[38] Junge, O. & Koltai, P. (2009) Discretization of the Frobenius–Perron operator using a Sparse Haar tensor basis: The Sparse Ulam method. *SIAM J. Numer. Anal.* **47** (5), 3464–3485.
[39] Keller, J., Franssen, H.-J. & Nowak, W. (2021) Investigating the pilot point ensemble Kalman filter for geostatistical inversion and data assimilation. *Adv. Water Resour.* **155**, 104010.
[40] Kim, D., Sra, S. & Dhillon, I. S. (2012) A non-monotonic method for large-scale non-negative least squares. *Optim. Method. Softw. (OMS)* **28**(5), 1012–1039.
[41] Kim, H. & Park, H. (2007) Sparse non-negative matrix factorizations via alternating non-negativity-constrained least squares for microarray data analysis. *Bioinformatics* **23** (12), 1495–1502.
[42] Kiplagat, J., Tran, D. N., Barber, T., *et al.* (2022) How health systems can adapt to a population ageing with HIV and comorbid disease. *Lancet HIV* **9** (4), e281–e292.
[43] Klus, S. (2020) Data-driven analysis of complex dynamical systems, Habilitation thesis, Freie Universität, Berlin. DOI: 10.17169/refubium-28554.
[44] Klus, S., Koltai, P. & Schütte, C. (2016) On the numerical approximation of the Perron-Frobenius and Koopman operator. *J. Comput. Dyn.* **3** (1), 51–79.

[45] Klus, S., Nüske, F., Koltai, P., *et al.* (2018) Data-driven model reduction and transfer operator approximation. *J. Nonlinear Sci.* **28**, 985–1010.

[46] Klus, S. & Schütte, C. (2016) Towards tensor-based methods for the numerical approximation of the Perron–Frobenius and Koopman operator. *J. Comput. Dyn.* **3** (2), 139–161.

[47] Kovachki, N. B. & Stuart, A. M. (2019) Ensemble Kalman inversion: A derivative-free technique for machine learning tasks. *Inverse Probl.* **35** (9), 095005.

[48] Kutz, J. N., Brunton, S. L., Brunton, B. W. & Proctor, J. L. (2016) *Dynamic Mode Decomposition: Data-Driven Modeling of Complex Systems*. Society for Industiral and Applied Mathematics.

[49] Kutz, J. N., Fu, X. & Brunton, S. L. (2016) Multiresolution dynamic mode decomposition. *SIAM J. Appl. Dyn. Syst.* **15** (2), 713–735.

[50] Lampe, M. A., Nesheim, S. R., Oladapo, K. L., Ewing, A. C., Wiener, J. & Kourtis, A. P. (2023) Achieving elimination of perinatal HIV in the United States. *Pediatrics* **151** (5), e2022059604.

[51] Lasota, A. & Mackey, M. C. (2013) *Chaos, Fractals, and Noise: Stochastic Aspects of Dynamics*, Vol. **97**, Springer Science & Business Media.

[52] Lawson, C. L. & Hanson, R. J. (1995) *Solving Least Squares Problems*, SIAM.

[53] Li, X.-Z., Yang, J. & Martcheva, M. (2020). *Age structured epidemic modeling*, Vol. **52**, Springer Nature.

[54] Li, Z. (2020) An iterative ensemble Kalman method for an inverse scattering problem in acoustics. *Mod. Phys. Lett. B* **34** (28), 2050312.

[55] Marcus, J. L., Leyden, W. A., Alexeeff, S. E., *et al.* (2020) *Comparison of overall and comorbidity-free life expectancy between insured adults with and without HIV infection, 2000 – 2016. JAMA Netw. Open* **3** (6), e207954–e207954.

[56] Mateen, F. J. & Mills, E. J. (2012) Aging and HIV-related cognitive loss. *JAMA* **308** (4), 349–350.

[57] Murray, J. D. & Murray, J. D. (2003) *Mathematical Biology I: An Introduction*, Vol. **18**, Springer.

[58] Nadisic, N., Cohen, J. E., Vandaele, A. & Gillis, N. (2022) Matrix-wise l0-constrained sparse nonnegative least squares. *Mach. Learn.* **111** (12), 4453–4495.

[59] Nanditha, N. G. A., Paiero, A., Tafessu, H. M., *et al.* (2021) Excess burden of age-associated comorbidities among people living with HIV in British Columbia, Canada: A population-based cohort study. *BMJ Open* **11** (1), e041734.

[60] Paul, R. H., Cooley, S. A., Garcia-Egan, P. M. & Ances, B. M. (2018) Cognitive performance and frailty in older HIV-positive adults. *JAIDS J. Acquir. Immune Defic. Syndr.* **79** (3), 375–380.

[61] Petoumenos, K. & Worm, S. W. (2011) HIV infection, aging and cardiovascular disease: epidemiology and prevention. *Sex. Health* **8** (4), 465–473.

[62] Proctor, J. L. & Eckhoff, P. A. (2015) Discovering dynamic patterns from infectious disease data using dynamic mode decomposition. *Hum. Res. Dev.* **7** (2), 139–145.

[63] Puglia, M. & Voller, F. (2024). HIV/AIDS in Toscana, Technical report, Osservatorio di epidemiologia - Azienda Regionale di Sanitá della Toscana.

[64] Rodes, B., Cadinanos, J., Esteban-Cantos, A., Rodríguez-Centeno, J. & Arribas, J. R. (2022) Ageing with HIV: Challenges and biomarkers. *eBioMedicine* **77**, 103896.

[65] Roomaney, R. A., van Wyk, B. & Pillay-van Wyk, V. (2022) Aging with HIV: Increased risk of HIV comorbidities in older adults. *Int. J. Environ. Res. Pub. Health* **19** (4), 2359.

[66] Schillings, C. & Stuart, A. M. (2017) Analysis of the ensemble Kalman filter for inverse problems. *SIAM J. Numer. Anal.* **55** (3), 1264–1290.

[67] Schmid, P. J. (2010) Dynamic mode decomposition of numerical and experimental data. *J. Fluid. Mech.* **656**, 5–28.

[68] Schwenzer, M., Visconti, G., Ay, M., Bergs, T., Herty, M. & Abel, D. (2020) Identifying trending coefficients with an ensemble Kalman filter. *IFAC-PapersOnLine* **53** (2), 2292–2298.

[69] Smith, L., Letendre, S., Erlandson, K. M., Ma, Q., Ellis, R. J. & Farhadian, S. F. (2022) Polypharmacy in older adults with HIV infection: Effects on the brain. *J. Am. Geriatr. Soc.* **70** (3), 924.

[70] Stover, J. & Glaubius, R. (2024) Methods and assumptions for estimating key hiv indicators in the unaids annual estimates process. *JAIDS J. Acquir. Immune Defic. Syndr.*, **95** (1S), e5–e12.

[71] Takeishi, N., Kawahara, Y. & Yairi, T. (2017) Sparse nonnegative dynamic mode decomposition. In *2017 IEEE International Conference on Image Processing (ICIP)*, IEEE, pp. 2682–2686.

[72] Trickey, A., Sabin, C. A., Burkholder, G., *et al.* (2023) Life expectancy after 2015 of adults with HIV on long-term antiretroviral therapy in Europe and North America: A collaborative analysis of cohort studies. *Lancet HIV* **10** (5), e295–e307.

[73] Van Benthem, M. H. & Keenan, M. R. (2004) Fast algorithm for the solution of large-scale non-negativity-constrained least squares problems. *J. Chemom.: A Journal of the Chemometrics Society* **18** (10), 441–450.

[74] Viguerie, A., Barros, G. F., Grave, M., Reali, A. & Coutinho, A. L. (2022) Coupled and uncoupled dynamic mode decomposition in multi-compartmental systems with applications to epidemiological and additive manufacturing problems. *Comput. Method. Appl. Mech. Eng.* **391**, 114600.

[75] Viguerie, A., Grave, M., Barros, G. F., Lorenzo, G., Reali, A. & Coutinho, A. L. (2022) Data-driven simulation of Fisher–Kolmogorov tumor growth models using dynamic mode decomposition. *J. Biomech. Eng.* **144** (12), 121001.

[76] Viguerie, A., O'Shea, J., Johnston, M., *et al.* (2025) Impact of increased uptake of long-acting injectable antiretroviral therapy on HIV incidence and viral suppression in the United States under 2021 FDA guidelines. *AIDS* **39** (8), 1024–1031.10.1097/QAD.0000000000004144.

[77] Viguerie, A., Song, R., Bosh, K., Lyles, C. M. & Farnham, P. G. (2022) Mortality among persons with HIV in the United States during the COVID-19 pandemic: A population-level analysis. *JAIDS J. Acquir. Immune Defic. Syndr.* **95** (2), 126–132.

[78] Viguerie, A., Song, R., Johnson, A. S., Lyles, C. M., Hernandez, A. & Farnham, P. G. (2023) Isolating the effect of COVID-19-related disruptions on HIV diagnoses in the United States in, 2020. *JAIDS J. Acquir. Immune Defic. Syndr.* **92** (4), 293–299.
[79] Viguerie, A., Song, R., Johnson, A. S., Lyles, C. M., Hernandez, A. & Farnham, P. G. (2024) COVID-19-related excess missed HIV diagnoses in the United States in, 2021. *AIDS* **38** (6), 907–911.
[80] Yegenoglu, A., Diaz, S., Krajsek, K. & Herty, M. (2020) Ensemble Kalman filter optimizing deep neural networks. In Conference on Machine Learning, Optimization and Data Science, Vol. **12514**, Springer LNCS Proceedings.

Appendix A. Full quantitative comparison with surveillance data

Table A1. *PWDH deaths by age bracket: surveillance vs simulation (2009–2022)*

Age bracket	Surveillance PWDH deaths	Simulated PWDH deaths	% Relative Error
Year 2009			
13–24	224	228	1.8
25–34	1339	1340	0.1
35–44	3953	3954	0.0
45–54	6565	6570	0.1
55–64	4093	4084	−0.2
65 +	1728	1782	3.1
Year 2010			
13–24	234	232	−0.9
25–34	1158	1158	0.0
35–44	3198	3197	−0.0
45–54	6202	6197	−0.1
55–64	4165	4157	−0.2
65 +	1683	1722	2.3
Year 2011			
13–24	225	226	0.4
25–34	1087	1084	−0.3
35–44	2846	2844	−0.1
45–54	5890	5895	0.1
55–64	4324	4330	0.1
65 +	1824	1875	2.8
Year 2012			
13–24	195	196	0.5
25–34	1110	1105	−0.5
35–44	2539	2539	0.0
45–54	5642	5642	0.0
55–64	4460	4480	0.4
65 +	1995	2010	0.8
Year 2013			
13–24	179	179	0.0
25–34	1053	1053	0.0
35–44	2294	2299	0.2
45–54	5447	5443	−0.1
55–64	4644	4640	−0.1
65 +	2239	2265	1.2

https://doi.org/10.1017/S0956792525100247 Published online by Cambridge University Press

Table A1. *(Continued)*

Age bracket	Surveillance PWDH deaths	Simulated PWDH deaths	% Relative Error
Year 2014			
13–24	186	183	−1.6
25–34	996	994	−0.2
35–44	2227	2220	−0.3
45–54	5141	5139	−0.0
55–64	5096	5095	−0.0
65 +	2450	2466	0.7
Year 2015			
13–24	161	162	0.6
25–34	994	993	−0.1
35–44	2029	2031	0.1
45–54	4909	4914	0.1
55–64	4986	4978	−0.2
65 +	2716	2733	0.6
Year 2016			
13–24	165	165	0.0
25–34	1098	1097	−0.1
35–44	1963	1968	0.3
45–54	4647	4643	−0.1
55–64	5380	5343	−0.7
65 +	3078	3127	1.6
Year 2017			
13–24	151	151	0.0
25–34	1045	1049	0.4
35–44	1831	1823	−0.4
45–54	4457	4457	0.0
55–64	5453	5457	0.1
65 +	3383	3389	0.2
Year 2018			
13–24	130	131	0.8
25–34	1034	1034	0.0
35–44	1775	1770	−0.3
45–54	4178	4176	−0.0
55–64	5444	5447	0.1
65 +	3631	3672	1.1
Year 2019			
13–24	135	132	−2.2
25–34	1100	1101	0.1
35–44	1783	1788	0.3
45–54	3642	3652	0.3
55–64	5581	5556	−0.5
65 +	4025	4056	0.8
Year 2020			
13–24	152	154	1.3
25–34	1265	1264	−0.1
35–44	2100	2096	−0.2
45–54	3871	3875	0.1
55–64	6501	6499	−0.0
65 +	5247	5304	1.1

https://doi.org/10.1017/S0956792525100247 Published online by Cambridge University Press

Table A1. *(Continued)*

Age bracket	Surveillance PWDH deaths	Simulated PWDH deaths	% Relative Error
Year 2021			
13–24	116	118	1.7
25–34	1405	1381	−1.7
35–44	2315	2310	−0.2
45–54	3895	3912	0.4
55–64	6827	6746	−1.2
65 +	5623	5673	0.9
Year 2022			
13–24	124	124	0.0
25–34	1388	1388	0.0
35–44	2399	2393	−0.3
45–54	3361	3341	−0.6
55–64	6110	6121	0.2
65 +	5555	5610	1.0

Appendix B. The Ensemble Kalman Inversion

The Ensemble Kalman Inversion (EKI) is a derivative-free iterative algorithm designed for solving inverse problems. It originates from the Ensemble Kalman Filter (EnKF), widely used in data assimilation, but is adapted to estimate parameters rather than states. The key idea is to evolve an ensemble of candidate solutions toward the minimiser of a least-squares functional by updating them with information from the data misfit.

A typical inverse problem in finite dimension reads as:

$$y = \mathscr{G}(u) + \eta \tag{B.1}$$

where $\mathscr{G}$ is the (possible nonlinear) forward operator between the finite dimensional spaces $X = \mathbb{R}^d$ and $Y = \mathbb{R}^k$ with $d, k \in \mathbb{N}$, $u \in X$ is the unknown parameter, $y \in Y$ is the observation and $\eta \sim \mathcal{N}(0, \Gamma)$ is the observational noise where Γ is a known covariance measurements, the observation and the mathematical model $\mathscr{G}$, we are interested in finding the corresponding control u. The EKI aims to solve a least–square formulation of the inverse problem and produces u^* such that

$$u^* = argmin_{u \in X} \frac{1}{2} ||\Gamma^{-\frac{1}{2}}(y - \mathscr{G}(u))||^2 \tag{B.2}$$

through a sequentially update of each member of an ensemble $k = 1, \ldots, K$ of elements u_k in the space X by means of the Kalman update formula, using the knowledge of the model $\mathscr{G}$ and given observational data y. The method is gradient free and even for small number of ensembles K satisfactory results have been reported. Assume a fixed value of $\lambda \in \Lambda$. The EnKF samples $J > 0$ initial values $u^{j,0}(\lambda) \in X$ and advances those according to the following equations. For a convergence analysis and stability properties we refer e.g. to [67]. Denote by $n \geq 0$ the iteration index and $\Delta t > 0$ an artificial time step. We indicate the set of ensembles by $U^n(\lambda) = \{u^n\}_{j=1}^J$. The set is propagated according to

$$u_j^{n+1} = u_j^n + C(U^n) \left(D(U^n) + \frac{1}{\Delta t} \Gamma^{-1} \right)^{-1} \left[y_j^{n+1} - \mathscr{G}(u^n) \right] \tag{B.3}$$

https://doi.org/10.1017/S0956792525100247 Published online by Cambridge University Press

where $C(U^n)$ and $D(U^n)$ are the covariance matrices depending on the ensemble set U^n at the iteration n and on $\mathscr{G}(U^n)$:

$$C(U^n) = \frac{1}{J}\sum_{j=1}^{J}(u_j^n - \bar{U}^n) \otimes (\mathscr{G}(u_j^n) - \bar{\mathscr{G}}), \tag{B.4}$$

$$D(U^n) = \frac{1}{J}\sum_{j=1}^{J}\left[\mathscr{G}(u_j^n) - \bar{\mathscr{G}}\right] \otimes \left[\mathscr{G}(u_j^n) - \bar{\mathscr{G}}\right], \tag{B.5}$$

$$\bar{U}^n := \frac{1}{J}\sum_{k=1}^{J} u_j^n,\ \bar{\mathscr{G}} := \frac{1}{J}\sum_{k=1}^{J}\mathscr{G}(u_j^n). \tag{B.6}$$

Convergence results can be found in [67, 34, 33] and the reference therein.

Cite this article: Viguerie A and Iacomini E. Ageing and mortality of persons with HIV: a novel data-driven approach. *European Journal of Applied Mathematics*, https://doi.org/10.1017/S0956792525100247